

Space: Science & Technology

Determining Maximum Allowable Current of an RBS using a Directed Graph Model and Greedy Algorithm --Manuscript Draft--

Manuscript Number:	SPACE-D-23-00082R2
Full Title:	Determining Maximum Allowable Current of an RBS using a Directed Graph Model and Greedy Algorithm
Short Title:	
Article Type:	Research Article
Section/Category:	Space Technology
Keywords:	Reconfigurable Battery System; Maximum Allowable Current; Directed Graph Model; Greedy Algorithm
Corresponding Author:	Cheng Qian CHINA
Corresponding Author Secondary Information:	
Corresponding Author's Institution:	
Order of Authors:	Binghui Xu Guangbin Hua Cheng Qian Quan Xia Bo Sun Yi Ren Zili Wang
Order of Authors Secondary Information:	
Manuscript Region of Origin:	CHINA
Abstract:	Reconfigurable battery systems provide a promising alternative to traditional battery systems due to their flexible and dynamically changeable topological structures that can be adapted to different battery charging and discharging strategies. A critical system parameter known as the maximum allowable current (MAC) is pivotal to RBS operation. This parameter is instrumental in maintaining the current of each individual battery within a safe range and serves as a guiding indicator for the system's reconfiguration, ensuring its safety and reliability. This paper proposes a method for calculating the MAC of an arbitrary RBS using a greedy algorithm in conjunction with a directed graph model of the RBS. Using the shortest path of the battery, the greedy algorithm transforms the exhaustion of the switch states in the brute-force algorithm or variable search without utilizing structures in the heuristic algorithms in the combination of the shortest paths. The directed graph model, based on an equivalent circuit, provides a specific method for calculating the MAC of a given structure. The proposed method is validated using two previously published RBS structures and an additional one with a more complex structure. The results are the same as those from the brute-force algorithm, but the proposed method significantly improves the computational efficiency, being theoretically $N_s^2 \cdot N_b \cdot \log_{10} N_b$ times faster than the brute-force algorithm for an RBS with N_b batteries and N_s switches. Another advantage of the proposed method is its ability to calculate the MAC of RBSs with arbitrary structures and variable batteries, even in scenarios with random isolated batteries.
Suggested Reviewers:	

Opposed Reviewers:	
Additional Information:	
Question	Response
Authorship As corresponding author, I confirm that all authors have: <ul style="list-style-type: none"> • Seen and approved the submitted manuscript and all related materials. • Agreed to be listed as an author and agreed to the submitted order of authorship. <p>(We will verify this requirement with all co-authors upon submission. Non-compliance may lead to rejection.)</p>	Yes

Dear Dr. Tian and the anonymous reviewers,

On behalf of my co-authors, we express our sincere gratitude for providing us with the opportunity to revise our manuscript. We highly value the reviewers' insightful and constructive comments and suggestions on our manuscript titled "Maximum Allowable Current Determination of RBS By Using a Directed Graph Model and Greedy Algorithm" (ID:SPACE-D-23-00082).

We have thoroughly examined the reviewers' comments and have made revisions, which are indicated in red and blue within the paper. Please find attached the revised version, which we kindly request you to consider.

There are two additional modifications that require attention. (1) The title of the paper has been revised to "Determining Maximum Allowable Current of an RBS using a Directed Graph Model and Greedy Algorithm". (2) The funding information has been omitted from the paper.

We would like to extend our great appreciation to you and the reviewers for their valuable feedback on our paper. We eagerly await your response.

Thank you and best regards.

Dr. Cheng Qian, on behalf of all authors

Beihang University

2023.11.10

Authors' Response to Reviewer 1

Comment 1:

Grammatical and spelling errors are still observed. Please check and fix carefully.

Response:

We apologize for our oversight regarding the grammatical and spelling errors, and we have thoroughly reviewed the manuscript and rectified them. Additionally, the manuscript has undergone revisions by a professional organization to ensure the accuracy of grammar and spelling.

Comment 2:

Since authors stated that there is no existing works on the MAC determination of RBSs that they could compare their solution with. So how the authors validate their works and their results.

Response:

To address the concern raised by the reviewer, we have incorporated a comprehensive discussion in the Case study section, specifically titled "Result validation". In this part, we thoroughly examine the correctness of the results obtained through the proposed greedy algorithm from two distinct perspectives: circuit analysis and validation against the brute-force algorithm. Additionally, we have included a comparison between the proposed greedy algorithm and two heuristic algorithms, namely simulated annealing and genetic algorithm, in the revised manuscript. There is a reference (No. 35 in the manuscript) claiming that the path selection problem under consideration may be NP-hard. Therefore, it is reasonable to compare the performance of the proposed greedy algorithm with these heuristic approaches, which are commonly employed to tackle NP-hard problems. Remarkably, our results demonstrate that the proposed

greedy algorithm consistently achieves the same or superior outcomes compared to the heuristic algorithms.

Here is the specific modification we made in the "Discussion":

The correctness of the outcomes provided by the proposed greedy algorithm will now be discussed from two perspectives: circuit analysis and validation against the brute-force algorithm. The result of the four-battery RBS structure shown in Fig. 4c is determined as an example. When B_1 and B_2 or B_3 and B_4 are connected in parallel, the RBS produces the maximum current, which is $\eta = 2$ (i.e., twice the current output of a single battery in the RBS). Adding more batteries to the main circuit only creates a series structure and does not improve the MAC. Therefore, the switch-control scheme provided in Tab. 4 maximizes the RBS output current. The brute-force method, which examines all possible switch states, yields the same η . This indicates that the proposed greedy algorithm successfully identifies the MAC among all the potential reconfigured structures.

And here is one of the comparisons between the proposed greedy algorithm and the heuristic algorithms in the "Result" section:

To verify and compare the proposed greedy algorithm, we also used the brute-force algorithm, which iterates through all possible switch states, and the heuristic algorithms (SA and GA) to calculate the MACs of the same RBSs. The final results of the brute-force algorithm are the same as those of the greedy algorithm and are shown in Tabs. 2, 3, and 4. However, the brute-force algorithm counts all possible switch states, which equates to 2^{15} , 2^{13} , and 2^{19} structures, respectively. The temporal evolutions of the objective values of the two heuristic algorithms during the iteration process are shown in Figs. 7a, 7b, and 7c, respectively, and compared with the proposed greedy algorithm. Compared with the SA and GA, the proposed greedy algorithm identifies the correct results within fewer iteration steps.

For more information on the other compared results and details, please refer to the revised "Case Study" section.

We hope that the reviewer is satisfied with the modifications made to the manuscript.

Comment 3:

Refer to the mentioned article as previously stated in comment 8 of the first revision.

Response:

We have reconsidered and modified the corresponding content about the analysis on MAC problem in the introduction. The mentioned article becomes important to this paper, therefore, we have cited it in the introduction and accept the reviewer's suggestion.

We have reevaluated and revised the relevant content regarding the analysis of the MAC problem in the introduction. The mentioned article holds significance in this paper, hence we have referenced it in the introduction and acknowledged the suggestion made by the reviewer.

Here is the specific modification we made in the introduction:

However, few studies have directly determined the MACs of RBSs, primarily due to the complexity arising from reconfiguration. In the field of computer science, there is a similar problem with scheduling tasks on dynamically reconfigurable hardware with limited resources and task interdependencies. This problem is analogous to the determination of the MAC and a corresponding solution has been proposed [33, 34]. However, dealing with the structural characteristics and circuit equations of RBSs is challenging for this method.

Authors' Response to Reviewer 2

Comment 1:

The latest related works need to be reviewed carfully please, expecially the works published in recent year 2022,2023.

Response:

We concur with the reviewer's assertion that it is important for our paper to undergo a thorough review of the most recent relevant literature. We have carefully scrutinized the pertinent works from the past five years and made appropriate revisions to the manuscript. In the "Introduction" section, we provide an overview of the challenges posed by the complex RBS structures in hardware design. Furthermore, the estimation and control of the system state of RBSs have been receiving increasing attention in recent time. Consequently, we have chosen several corresponding methodologies aimed at optimizing the system's performance.

Here is the specific modification in the introduction:

These complex structures between batteries and switches provide flexibility to RBSs but also pose challenges in hardware design. During the reconfiguration process, current deviation and fluctuation may occur. Specifically, when the system switches from series to parallel connection, a circulating current between parallel cells can be triggered due to a voltage imbalance [20]. Failure to fully consider this issue during the design of RBSs can result in damage to the batteries, switches, and wires. For example, Engelhardt et al. [21] applied an RBS to a fast-charging scenario with adaptive cell switching to balance cell states while adhering to voltage requests. However, the switching of batteries leads to intolerable current variations. To address this problem, Han et al. [22] derived an analytical expression for the maximum switch current during battery system reconfiguration. This analytical expression aids in the selection of switches and supports general hardware design. Recently, increasing attention has been paid to the estimation

and control of RBS system states, and several approaches have been proposed to optimize the performance of these systems. State estimation, which is an essential technology in traditional battery management systems, serves as the foundation for system control and holds great potential in the context of RBSs [23]. Couto et al. [24] introduced a partition-based unscented Kalman filter to estimate the state of a large-scale RBS, utilizing an enhanced reduced-order electrochemical model. Kersten et al. [25] utilized the balancing current of neighboring cells in parallel operation to determine the battery impedance, thereby obtaining information about the state of health and power capability of the RBS. Schmid et al. [26] further leveraged the reconfigurable nature of the system to actively diagnose faults, employing an algorithm that changes the system structure to enhance the fault isolability. Another active research area is the development of effective control strategies for RBSs to achieve optimal performance, including improved stability [27] and efficiency [28]. Han et al. [29] proposed a near-fastest battery balancing algorithm to minimize the time required for battery charge equalization. Liu et al. [30] also proposed a scheme for maximizing capacity utilization based on a path planning algorithm, aiming to enhance the battery consistency within the system. To break through the bottleneck of the potential short-circuit paths increasing exponentially with the RBS scale, Chen et al. [31] proposed a systematic approach based on sneak circuit theory. They conducted a comprehensive analysis of all paths between the cathode and anode of each battery in the RBS, identifying paths that consist only of switches as short-circuit paths for pre-checking before system reconfiguration. Artificial intelligence has also appeared in RBS management [32]. The effectiveness of the deep reinforcement learning method has been validated in real-world RBSs [28].

Comment 2:

The greedy algorithm and the brute force algorithm are compared in this paper, but the advantages and disadvantages of this algorithm compared with other algorithms cannot be determined.

Response:

Thanks to the suggestion of the reviewer! We have revised the "Discussion" subsection and included a specific part to analyze the advantages and disadvantages of the proposed greedy algorithm in comparison to other algorithms. Based on our discussion and comparison, the proposed greedy algorithm demonstrates a significant advantage in terms of its effectiveness and efficiency. It is also capable of handling RBSs with diverse structures. However, this algorithm may encounter challenges when dealing with large-scale problems due to its exponential time complexity. Furthermore, the simplification of the derivation by assuming that all batteries are identical may introduce a slight bias to the MAC due to variations in open-circuit voltage u_b and internal resistance r_b in reality. We have also provided a solution to address this issue.

The relevant content has been added to the "Pros and cons analysis" part within the "Discussion" subsection. Once again, we appreciate this constructive comment from the reviewer.

Comment 3:

This paper mainly applies to the four-battery system, but the usability of other structures of RBS should also be discussed.

Response:

Thanks for the valuable feedback. We have thoroughly considered the comment made by the reviewer. In response, we have supplemented the case study with a series of experiments on RBSs with variant batteries. Overall, the proposed greedy algorithm

has been applied to RBSs with three different structures, variant batteries, and scenarios involving random isolated batteries. The correctness and efficiency of the proposed greedy algorithm have been verified through the comparison with other algorithms.

The relevant content has been added to the "Case study" section. We hope it can address the reviewer's concerns.

1 Determining Maximum Allowable Current of an RBS using a
 2 Directed Graph Model and Greedy Algorithm

3 Binghui Xu^{1†}, Guangbin Hua^{1†}, Cheng Qian^{1*}, Quan Xia^{1,2}, Bo Sun¹, Yi Ren¹, and
 4 Zili Wang¹

5 ¹School of Reliability and Systems Engineering, Beihang University, Beijing, 100191,
 6 China

7 ²School of Aeronautic Science and Engineering at Beihang University, Beijing, China

8 *Address correspondence to: cqian@buaa.edu.cn

9 [†]These authors contributed equally to this work.

10

Abstract

11

Reconfigurable battery systems (~~RBSs~~) present provide a promising alternative to traditional battery systems due to their flexible and dynamically changeable topological ~~structure structures~~ that can be adapted to different battery charging and discharging strategies. During ~~RBS operation, a~~ A critical system parameter known as the maximum allowable current (MAC) ~~become pivotal is pivotal to RBS operation~~. This parameter is instrumental in maintaining the current of each individual battery within a safe range and serves as a guiding indicator for the system's reconfiguration, ~~thereby~~ ensuring its safety and reliability. This paper proposes a method ~~to calculate for calculating~~ the MAC of ~~arbitrary RBSs~~ ~~an arbitrary RBS~~ using a greedy algorithm in conjunction with a directed graph model of the RBS. By introducing Using the shortest path of the battery, the greedy algorithm transforms the ~~enumeration of exhaustion of the~~ switch states in the brute-force algorithm ~~into the or variable search without utilizing structures in the heuristic algorithms in the~~ combination of the shortest paths; ~~which greatly increases the efficiency with which the MAC is determined~~. The directed graph model, based on ~~the an~~ equivalent circuit, provides a specific method for calculating the MAC of a given structure. The proposed method is validated ~~on two published four-battery RBSs and using two previously published RBS structures and an additional~~ one with a more complex structure. The results are the same as those ~~of from~~ the brute-force algorithm, but the proposed method significantly improves the computational efficiency ($N_s 2^{N_s - N_b} \log_{10} N_b$, being theoretically $N_s 2^{N_s - N_b} \log_{10} N_b$ times faster than the ~~brute force brute force~~ algorithm for an RBS with N_b batteries and N_s switches, ~~theoretically~~). The main ~~Another~~ advantage of the proposed method is its ability to calculate the MAC of RBSs with arbitrary structures ~~and variable batteries~~, even in scenarios with random isolated batteries.

33 1 Introduction

34 Battery energy storage systems (BESSs) are ~~extensively used widely utilized~~ in various applications
35 [1], such as wind power plants [2] and space power systems [3, 4], ~~to store and release for the purpose~~
36 ~~of storing and releasing~~ high-quality electrical energy [5]. Typically, a BESS consists of numerous
37 batteries interconnected by series-parallel circuitry to provide the required ~~capacity storage storage~~
38 ~~capacity~~. However, ~~traditional conventional~~ BESSs, in which the batteries are connected in a fixed
39 topology, suffer from a significant weakness in their worst ~~battery batteries~~ due to the so-called
40 cask effect. ~~Moreover Furthermore~~, if the worst battery fails during operation, it is highly likely
41 to ~~exacerbate accelerate~~ the degradation of the other batteries, ~~leading to resulting in~~ reliability
42 and safety issues ~~at the system level~~ [6, 7, 8]. These ~~problems have become significant technical~~
43 ~~barriers challenges have become major technical obstacles~~ in many engineering projects ~~requiring~~
44 ~~that demand~~ high reliability, such as ~~developing new generation the development of next-generation~~
45 space vehicles [9].

46 Reconfigurable battery systems (RBSs), which can dynamically switch ~~as required to between~~
47 different circuit topologies ~~as needed~~, are expected to ~~solve this problem~~ [10]. The switching circuit
48 ~~helps to isolate unhealthy batteries, thereby improving the safety and reliability of the battery~~
49 ~~system. To illustrate the working principle of an RBS, we consider be able to address these issues~~
50 ~~[10]. In a typical RBS structure developed by Visairo [11] (Fig. ??), which is taken as an example~~
51 ~~to show the reconfiguration process. In this structure, the batteries can be connected not only in~~
52 ~~series when the switches $S_1, S_5, S_6, S_7, S_8, S_9$, and S_{13} are closed (see Fig. ??) but also in parallel~~
53 ~~when $S_1, S_2, S_3, S_4, S_5, S_9, S_{10}, S_{11}, S_{12}$, and S_{13} are closed (Fig. ??). Furthermore, when an~~
54 ~~unhealthy battery, for instance, the orange one B_3 in Fig. ??, appears in the RBS, it additional~~
55 ~~switches are introduced between the batteries to form a reconfigurable network, where the circuit's~~
56 ~~topology can be altered by opening or closing the switches. By opening the switches adjacent to~~
57 ~~the unhealthy batteries, they~~ can be isolated ~~by opening its two adjacent switches (i.e., S_4 and~~
58 ~~S_{11}), from the system, ensuring that the system remains in a reliable working mode. operational~~
59 ~~state [12]. Furthermore, an RBS can be reconfigured to adapt to different charging and discharging~~
60 ~~strategies, thereby enhancing the system's efficiency and prolonging the battery's lifespan [13]. These~~
61 ~~advantages make RBSs a promising alternative to traditional BESSs.~~

62 ————— (a) The RBS structure proposed by Visairo[11], with all batteries in (b) series
63 connection, (c) parallel connection, and (d) battery B_3 isolated.

64 Recently, various types of RBSs with different ~~The early research on RBSs mainly focused on the~~
65 ~~topological design of their structures, incorporating different levels of flexibility and reconfigurability~~
66 ~~have been designed~~ to meet application requirements. For example, Ci et al. [14] proposed an
67 RBS structure that dynamically adjusts the battery discharge rate to fully exploit the available
68 capacity of each battery. Jan 's [15, 16] ~~structures reconfigure structures~~ et al. [15, 16] designed
69 ~~structures that reconfigure circuits~~ with variant batteries in series to ~~reach the (constantly changing~~
70 ~~) accommodate the constantly changing~~ voltage requirements during electric vehicle charging. As
71 shown in Fig. ??, the ~~A~~ structure proposed by Visairo et al. [11] changes ~~and Kumar [11]~~ alters
72 the system's output voltage based on the load conditions, thereby reducing ~~the power loss of power~~

73 loss in the voltage regulator during the power supply process and improving the efficiency of energy
74 use. Also, to enhance the energy efficiency of the system, Lawson et al. enhancing energy efficiency.
75 Lawson [17] and He et al. [18] also focused on enhancing energy efficiency, and proposed simplified
76 structures that have fewer switches than Visairo's design the design of Visairo and Kumar. Kim et
77 al. [19] improved the system's ability ability of an RBS structure to recover from battery failures by
78 introducing multiple portsinto the structure.

79 The complex structure . These complex structures between batteries and switches gives RBSs
80 flexibility but also creates challenges in the designand control of the system . Thus, several approaches
81 to analyze the RBS structure and performance have been proposed to tackle these challenges.
82 For instance, provide flexibility to RBSs but also pose challenges in hardware design. During
83 the reconfiguration process, current deviation and fluctuation may occur. Specifically, when the
84 system switches from series to parallel connection, a circulating current between parallel cells can
85 be triggered due to a voltage imbalance [20]. Failure to fully consider this issue during the design
86 of RBSs can result in damage to the batteries, switches, and wires. For example, Engelhardt et al.
87 [21] applied an RBS to a fast-charging scenario with adaptive cell switching to balance cell states
88 while adhering to voltage requests. However, the switching of batteries leads to intolerable current
89 variations. To address this problem, Han et al. [22] derived an analytical expression for the maxi-
90 mum switch current during battery system reconfigurationfor a specific RBS structure. This helps
91 guide . This analytical expression aids in the selection of switches and supports the designof RBS
92 hardware—general hardware design.

93 Recently, increasing attention has been paid to the estimation and control of RBS system states,
94 and several approaches have been proposed to optimize the performance of these systems. State
95 estimation, which is an essential technology in traditional battery management systems, serves as
96 the foundation for system control and holds great potential in the context of RBSs [23]. Couto et al.
97 [24] introduced a partition-based unscented Kalman filter to estimate the state of a large-scale RBS,
98 utilizing an enhanced reduced-order electrochemical model. Kersten et al. [25] utilized the balancing
99 current of neighboring cells in parallel operation to determine the battery impedance, thereby
100 obtaining information about the state of health and power capability of the RBS. Schmid et al. [26]
101 further leveraged the reconfigurable nature of the system to actively diagnose faults, employing an
102 algorithm that changes the system structure to enhance the fault isolability. Another active research
103 area is the development of effective control strategies for RBSs to achieve optimal performance,
104 including improved stability [27] and efficiency [28]. Han et al. [29] proposed a near-fastest battery
105 balancing algorithm to minimize the time required for battery charge equalization. Liu et al. [30]
106 also proposed a scheme for maximizing capacity utilization based on a path planning algorithm,
107 aiming to enhance the battery consistency within the system. To break through the bottleneck of
108 the potential short-circuit paths increasing exponentially with the RBS scale, Chen et al. [31] pro-
109 posed a systematic approach based on sneak circuit theoryto fundamentally avoid the short-circuit
110 problem of RBSs: They thoroughly analyzed . They conducted a comprehensive analysis of all paths
111 between the cathode and anode of each battery in the RBSand identified paths that only contain .
112 identifying paths that consist only of switches as short-circuit paths for pre-checking before system
113 reconfiguration. Artificial intelligence has also appeared in RBS management [32]. The effectiveness

114 of the deep reinforcement learning method has been validated in real-world RBSs [28].

115 In spite of the maximum switch current mentioned above, the maximum The maximum allowable
116 current (MAC), which is defined as the maximum allowed current under current allowed within the
117 constraints of the a battery cell, is another critical a crucial indicator of RBSs that needs need to be
118 evaluated during the design or and control of the system. The MAC helps the designers assess assists
119 designers in assessing whether the RBS meets the output current requirements and contributes to the
120 formulation development of appropriate and safe management strategies for the battery management
121 system. Unfortunately However, few studies have analyzed the RBS structure to determine the
122 RBS MAC. An intuitive and straightforward method is to enumerate all possible switch states and
123 calculate the output current of directly determined the MACs of RBSs, primarily due to the system
124 under each reconfigured structure complexity arising from reconfiguration. In the field of computer
125 science, there is a similar problem with scheduling tasks on dynamically reconfigurable hardware
126 with limited resources and task interdependencies. This problem is analogous to the determination
127 of the MAC and a corresponding solution has been proposed [33, 34]. However, dealing with the
128 structural characteristics and circuit equations of RBSs is challenging for this method. From the
129 perspective of RBS structure analysis, the MAC problem can be transformed into a problem of
130 finding the maximum output current among all possible reconfigurations of the RBS. However, this
131 method is inefficient and time-consuming, especially for RBSs with a large number of switches. may
132 be an NP-hard problem [35]. Common methods such as brute-force algorithms, simulated annealing
133 (SA) algorithms, and genetic algorithms (GA) have the drawbacks of inefficiency, excessive time
134 consumption, and an inability to guarantee the globally optimal solution.

135 To solve this issue, this paper proposes an efficient method to evaluate the MAC MACs of RBSs.
136 In this method, a greedy algorithm is designed to efficiently search the possible circuit topology of
137 RBSs with MAC topologies of RBSs. This algorithm transforms the enumeration of switch states in
138 the brute-force algorithm into the combination of the batteries' shortest paths. An improved direct
139 graph model that considers the inefficient search for reconfigurations into a proactive combining of
140 the shortest paths of the batteries. Furthermore, an improved directed graph model is introduced
141 to analyze the current of the RBS, taking into account factors such as the voltage, the internal
142 resistance, the MAC of the battery, and the external load is also introduced to analyze the current of
143 the RBS. external load. The main contributions of this paper study can be summarized as follows:

- 144 • An efficient method is proposed to determine the MAC MACs of RBSs with arbitrary struc-
145 tures, including scenarios with isolated batteries.
- 146 • A greedy algorithm is applied to solve the MAC problem, the computational complexity of
147 which is greatly reduced compared with the brute-force algorithm.
- 148 • An improved directed graph model is introduced to provide a specific method for calculating
149 the MAC of a given structure.

150 The remainder of this paper is organized as follows: Section II presents the framework and
151 details of the proposed directed graph model and the greedy algorithm. Section III discusses a case
152 study that uses applies the proposed method to determine the MACs of two published four-battery

153 RBSs and RBS structures and a new one with a more complex structure. The calculation results,
 154 the algorithm's computational complexity computational complexity of the algorithm, and scenarios
 155 such as battery random isolation are also discussed. Finally, the concluding remarks are presented
 156 in Section IV.

157 2 Methodology

158 The central principle of this the proposed method is to connect the batteries in an RBS in parallel to
 159 the extent possible maximum possible extent, thereby maximizing the output current of the RBS. To
 160 achieve this universally and automatically, the overall process is divided into the four steps shown
 161 in Fig. 1. First, a directed graph model is established for the subsequent computations. The model
 162 not only contains the connected relationships between batteries and switches but also retains the
 163 performance parameters of the batteries. Subsequently, based on the equivalent circuit, the MAC
 164 problem is transformed into specific objective functions and constraints. The shortest paths (SPs,
 165 where additional batteries and switches on the path are penalized as distance) for for distance of
 166 the batteries are then obtained by using the Dijkstra algorithm to connect the batteries in the RBS
 167 in parallel. Finally, a greedy algorithm is used to organize the switches, allowing the batteries to
 168 connect via their SPs while satisfying the constraints, resulting in the MAC of the RBS.

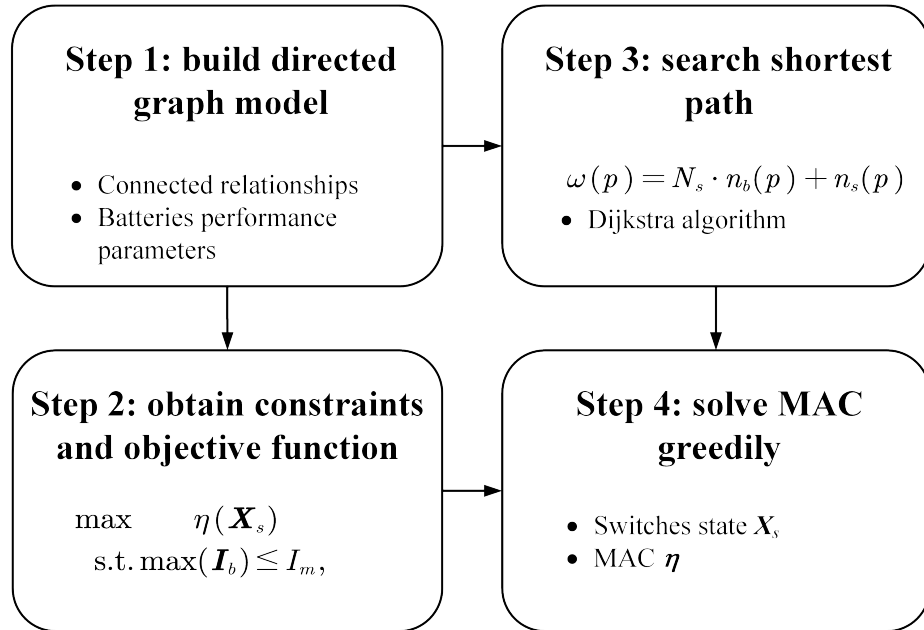


Figure 1: Diagram A diagram of this the proposed method, which contains four main steps.

169 2.1 Directed graph model

170 He et al. [36] proposed an abstracted directed graph model for an RBS, where the nodes represent
 171 the batteries, the edges represent the configuration flexibility, and the weight of each vertex

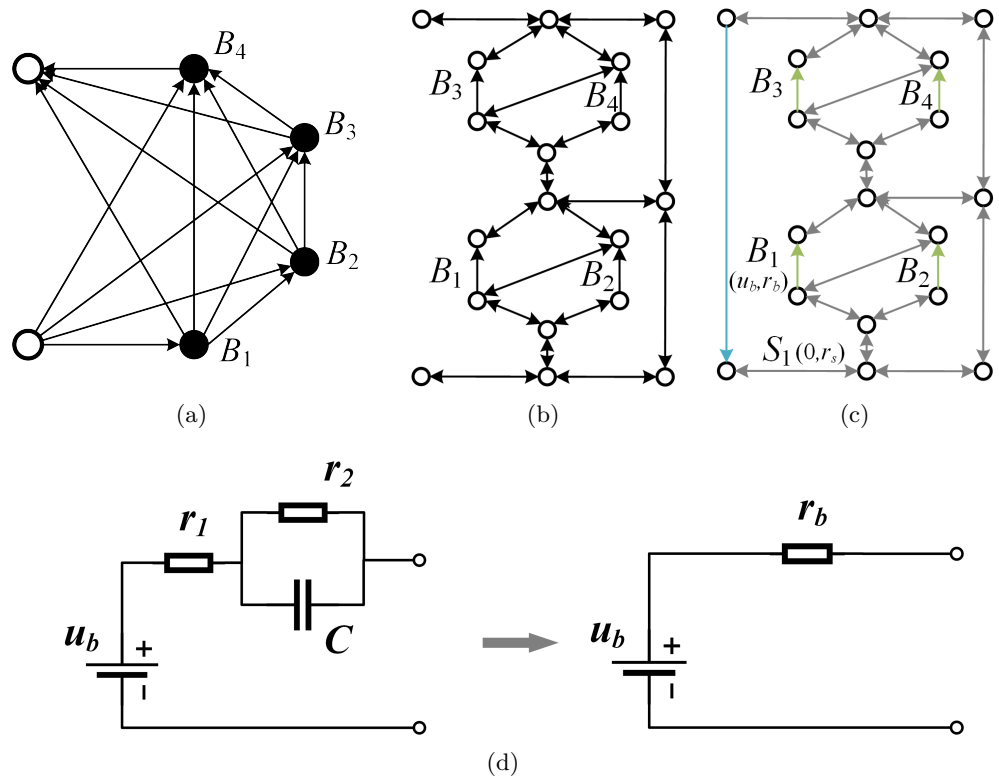


Figure 2: ~~Directed~~ The directed graph models used in (a) He's the work of He et al. [36], (b) our previous work, and (c) the improved model in this paper. (d) The equivalent circuit of a battery in this method.

corresponds to the battery voltage (Fig. 2a). The model captures all potential system configurations and offers a direct metric for configuration flexibility, but it does not specify the physical implementation of the connectivity between batteries, meaning that one graph might correspond to multiple RBS structures. We previously proposed a directed graph model that differs ~~completely from He significantly from He et al.~~'s model by using nodes to represent the connections between batteries and switches and directed edges to represent batteries and switches (Fig. 2b), allowing for a one-to-one correspondence between ~~the an~~ RBS structure and ~~the its~~ directed graph model. This model accurately and comprehensively represents the RBS topological structure but cannot be used for quantitative MAC calculations because it does not consider the voltage, internal resistance, ~~and or~~ MAC of the battery. To address this issue, we improve our previous model by adding electromotive force and resistance attributes on the edges based on ~~its the corresponding~~ equivalent circuits. The model also considers the external load as an equivalent resistance and integrates it into the analysis, making it a complete circuit model for later circuit ~~analyses analysis~~. Fig. 2c shows the improved directed graph model used in this paper. The following provides a detailed explanation of the method used for equating components in RBSs and constructing the directed graph model.

To use circuit analysis methods to solve the MAC of the RBS, the components in the RBS are equated to ideal circuit elements. For instance, as shown in Fig. 2d, the battery in the RBS is represented as a black-box circuit consisting of two resistors r_1 and r_2 and a capacitor C , in what is known as the Thevenin model [37, 38]. With an emphasis on the stable output of the RBS, the capacitor in the Thevenin model can be considered as an open circuit without affecting the steady-state current. Therefore, battery B_i in the RBS can be simplified as a series connection between a constant voltage source u_i and a resistor r_i . Furthermore, the state of the switch S_j in the RBS is represented by a binary variable x_j , where 0 is ON and 1 is OFF. When the switch is closed, the circuit can be regarded as a resistor with a very small resistance r_j . Finally, the external load is considered as a resistor with resistance R_o .

For a given RBS structure, its directed graph model $G(V, E)$ is constructed as follows:

1. Nodes: The nodes in the directed graph correspond to the connection points of components in the actual RBS. Assuming there are a total of N nodes in the RBS, for the sake of convenience, the anode of the RBS is denoted as v_1 and the cathode as v_N .
2. Edges: The edges in the directed graph correspond to the batteries, switches, and external electrical loads in the actual RBS. Therefore, there are three types of directed edges. For battery B_i , its directed edge e_i is drawn from the cathode to the anode because the battery in operation only allows current to flow in one direction. For switch S_j , since it is allowed to work under bidirectional currents, it is represented by a pair of directed edges with two-way directions. ~~Regarding the external electronic~~ For the external electrical load, because it is connected to the anode and cathode of the RBS, a directed edge from v_N to v_1 ~~represents is used to represent~~ it. In conclusion, for a given RBS structure with N_b batteries and N_s switches, the number of directed edges is $N_b + 2N_s + 1$, where 1 ~~refers to~~ represents the external electrical load.
3. Attributes of edges: Each edge is assigned two attributes, a voltage difference and a resistance,

212 based on the equivalent method mentioned above. The values for battery B_i , switch S_j , and
 213 the external loads correspond to (u_i, r_i) , $(0, r_j)$, and $(0, R_o)$, respectively.

214 2.2 Constraints and objective function

215 For a given RBS, determining its-the MAC involves maximizing the RBS output current while
 216 ensuring that all battery currents do not exceed the batteries' MAC. This subsection establishes the
 217 constraints and objective function used to determine the RBS's-MAC through circuit analysis based
 218 on the directed graph model provided in the previous section.

219 First, the topology in the directed graph model is represented in matrix form the form of a matrix
 220 \mathbf{A} , which is known as the incidence matrix and is defined as follows:

$$a_{kl} = \begin{cases} 1, & \text{edge } l \text{ leaves node } k, \\ -1, & \text{edge } l \text{ enters node } k, \\ 0, & \text{otherwise.} \end{cases} \quad (1)$$

221 For a directed graph consisting of N nodes and $N_b + 2N_s + 1$ directed edges, its-the incidence
 222 matrix \mathbf{A} is an $N \times (N_b + 2N_s + 1)$ matrix. In this matrix, the rows and columns represent the
 223 nodes and edges of the directed graph, respectively. By distinguishing the components in the RBS
 224 corresponding to each column, \mathbf{A} can be rewritten as

$$\mathbf{A} = [\mathbf{A}_b \quad \mathbf{A}_s \quad \mathbf{A}_o], \quad (2)$$

225 where \mathbf{A}_b , \mathbf{A}_s , and \mathbf{A}_o are the submatrices corresponding to the batteries, switches, and external
 226 electrical load, respectively. To reduce the computational complexity, the dimensions of matrix \mathbf{A} are
 227 reduced. Since each directed edge has one node to leave and one to enter, the values in every column
 228 of \mathbf{A} sum to zero. Therefore, removing the last row will not result in a loss of information. Conversely,
 229 since each switch in the RBS is represented by a pair of directed edges with two-way directions, the
 230 two columns corresponding to the switch are mutually opposite. Thus, for the submatrix \mathbf{A}_s , only
 231 one column is retained for each pair of columns representing the same switch. As a result, \mathbf{A} can
 232 be reduced to an $(N - 1) \times (N_b + N_s + 1)$ matrix, denoted $\tilde{\mathbf{A}}$, for further calculation of the current
 233 and voltage. Similar to Eq. (2), $\tilde{\mathbf{A}}$ can be rewritten as

$$\tilde{\mathbf{A}} = [\tilde{\mathbf{A}}_b \quad \tilde{\mathbf{A}}_s \quad \tilde{\mathbf{A}}_o]. \quad (3)$$

234 After obtaining the incidence matrix, the currents of all batteries and output in the RBS are
 235 determined by solving the circuit equations. According to Kirchhoff's laws, we have

$$\begin{cases} \tilde{\mathbf{A}}\mathbf{I} = \mathbf{0}, \\ \mathbf{U} = \tilde{\mathbf{A}}^T \mathbf{U}_n, \end{cases} \quad (4)$$

236 where \mathbf{I} and \mathbf{U} indicate the current and voltage difference arrays of the $N_b + N_s + 1$ edges, respectively,

²³⁷ and \mathbf{U}_n is the voltage array of the $N - 1$ nodes. These directed edges are treated as generalized
²³⁸ branches and expressed in matrix form as follows:

$$\mathbf{I} = \mathbf{YXU} - \mathbf{YXU}_s + \mathbf{I}_s, \quad (5)$$

²³⁹ where \mathbf{U}_s and \mathbf{I}_s denote the source voltage and source current of the generalized branches, respec-
²⁴⁰ tively. Because all batteries have been made equivalent to voltage sources rather than current sources
²⁴¹ in the previous subsection, all elements of the array \mathbf{I}_s are zero, whereas the elements of the array
²⁴² \mathbf{U}_s are equal to the first attribute of the corresponding edges in the directed graph. The matrix \mathbf{Y} in
²⁴³ Eq. (5) is the admittance matrix of the circuit and is defined as the inverse of the impedance matrix.
²⁴⁴ The elements on the diagonal of matrix \mathbf{Y} are equal to the reciprocal of the resistance, which is the
²⁴⁵ second attribute of the corresponding edges in the directed graph. The off-diagonal elements of \mathbf{Y}
²⁴⁶ are zero. \mathbf{X} is the state matrix that determines whether the RBS batteries and switches can pass
²⁴⁷ current. It is defined as

$$\mathbf{X} = \text{diag}(\underbrace{1, 0, \dots, 1}_{N_b \text{ of } 0/1}, \underbrace{1, 0, \dots, 1}_{N_s \text{ of } 0/1}, 1) = \begin{bmatrix} \mathbf{X}_b & & \\ & \mathbf{X}_s & \\ & & 1 \end{bmatrix}, \quad (6)$$

²⁴⁸ where element x_i of matrix \mathbf{X}_b indicates whether battery B_i has been removed from the circuit, with
²⁴⁹ $x_i = 1$ indicating removal and $x_i = 0$ indicating that battery B_i is still available to supply power.
²⁵⁰ When all batteries are healthy and capable of providing current to the external load, \mathbf{X}_b is the
²⁵¹ identity matrix. The elements x_j of matrix \mathbf{X}_s determine whether switch S_j is closed, with $x_j = 1$
²⁵² indicating a closed switch and $x_j = 0$ indicating an open switch, which is consistent consistently
²⁵³ with the previous subsection.

²⁵⁴ Theoretically, the output current I_o and the currents of each battery \mathbf{I}_b in the RBS can be
²⁵⁵ determined by solving Eqs. (4)–(6) under any given state \mathbf{X} . To further simplify the problem, it
²⁵⁶ is assumed that all batteries have the same electromotive force and internal resistance, which are
²⁵⁷ denoted u_b and r_b , respectively. This allows us to derive explicit expressions for I_o and \mathbf{I}_b . After
²⁵⁸ derivation and simplification, the output current I_o and the currents of each battery \mathbf{I}_b are ultimately
²⁵⁹ represented as in Eqs. (7) and (8), respectively:

$$I_o = \frac{1}{R_o r_b} \tilde{\mathbf{A}}_o^T \mathbf{Y}_n^{-1}(\mathbf{X}) \tilde{\mathbf{A}}_b \mathbf{U}_b, \quad (7)$$

$$\mathbf{I}_b = \frac{1}{r_b^2} [\tilde{\mathbf{A}}_b^T \mathbf{Y}_n^{-1}(\mathbf{X}) \tilde{\mathbf{A}}_b \mathbf{U}_b - r_b \mathbf{U}_b], \quad (8)$$

²⁶⁰ where \mathbf{U}_b is an $N_b \times 1$ array with all elements equal to u_b , and \mathbf{Y}_n is the equivalent admittance
²⁶¹ matrix of the circuit and is defined as

$$\mathbf{Y}_n(\mathbf{X}) = \frac{1}{R_o} \tilde{\mathbf{A}}_o \tilde{\mathbf{A}}_o^T + \frac{1}{r_b} \tilde{\mathbf{A}}_b \mathbf{X}_b \tilde{\mathbf{A}}_b^T + \frac{1}{r_s} \tilde{\mathbf{A}}_s \mathbf{X}_s \tilde{\mathbf{A}}_s^T. \quad (9)$$

²⁶² To characterize the current output capacity of the RBS structure under different switching states,

264 an indicator η is defined by the ratio of I_o to $\max(\mathbf{I}_b)$:

$$\eta = \frac{I_o}{\max(\mathbf{I}_b)}. \quad (10)$$

265 Finally, the problem of finding the MAC can be formulated as

$$\max \eta(\mathbf{X}_s) \quad (11)$$

$$\text{s.t. } \max(\mathbf{I}_b) \leq I_m, \quad (12)$$

266 where I_m is the MAC of the battery.

267 However, it remains computationally difficult to solve Eq. (11) because of \mathbf{Y}_n^{-1} . 268 ~~On-one hand~~Firstly, the introduction of nonlinear terms ~~by-through~~ \mathbf{Y}_n^{-1} renders many methods in linear 269 optimization unsuitable for this problem. ~~On-the-other-hand~~Secondly, the rank of \mathbf{Y}_n is proportional 270 to the number of batteries and switches, which can be very large for a large RBS, leading to a significant 271 computational burden. As a result, intelligent algorithms that rely on evolution by iteration 272 may face efficiency problems when dealing with a large RBS. To address this issue, the problem 273 should be considered from the perspective of guiding the RBS to reconstruct as many parallel structures 274 as possible. Consequently, a greedy algorithm based on the shortest path is proposed. The 275 detailed implementation of this algorithm is presented in the following two subsections.

276 2.3 Shortest path

277 The path p used in this method is defined as the complete route that passes through one battery 278 (or a consecutive series of batteries) and closed switches, connecting the anode v_1 to the cathode v_N 279 of the RBS. By applying a penalty to the series-connected batteries on the path, where additional 280 batteries imply a greater distance, the algorithm encourages the RBS to form parallel structures to 281 the maximum extent possible. In addition, to reduce the number of switches controlled during the 282 reconstruction process, a penalty is also applied to the total number of switches on the path while 283 ensuring the minimum number of batteries. Therefore, the distance ω of path p is

$$\omega(p) = N_s n_b(p) + n_s(p), \quad (13)$$

284 where N_s is the total number of switches in the system, and $n_b(p)$ and $n_s(p)$ are the number of 285 batteries and switches in-along path p , respectively. Moreover, the shortest path SP_i is defined as 286 the path with the minimum ω for battery B_i :

$$SP_i = \arg \min_{p \in P_i} \omega(p), \quad (14)$$

287 where P_i is the set of all paths from v_1 to v_N that pass through directed edge i .

288 SP_i can be solved ~~by-using~~ the Dijkstra algorithm. The Dijkstra algorithm is a graph-search 289 method that finds the shortest path between two given nodes in a weighted graph, efficiently solving 290 the single-source shortest-path problem. Denoting the cathode and anode of battery B_i as v_i^- and

291 v_i^+ respectively, ~~then~~-path p of battery B_i can be divided into three segments: $v_1 \rightarrow v_i^-$, $v_i^+ \rightarrow v_N$,
 292 and $v_i^- \rightarrow v_i^+$. $v_i^- \rightarrow v_i^+$ is the directed edge corresponding to battery B_i . With the Dijkstra
 293 algorithm, ~~the~~ shortest paths for $v_1 \rightarrow v_i^-$ and $v_i^+ \rightarrow v_N$ can be calculated under the weights given
 294 in Eq. (13) and denoted $SP(v_i^- \rightarrow v_i^+)$ and $SP(v_i^+ \rightarrow v_N)$, respectively. Finally, SP_i for battery B_i
 295 is formed by the complete path, which consists of $SP(v_1 \rightarrow v_i^-)$, $v_i^- \rightarrow v_i^+$, and $SP(v_i^+ \rightarrow v_N)$.

296 2.4 Greedy algorithm

297 From the perspective of series vs. parallel connections, integrating more batteries into the circuit
 298 through their shortest paths (SPs) results in more batteries connected in parallel, thereby increasing
 299 the total output current of the RBS. However, conflicts may arise between the SPs of different
 300 batteries. For instance, the SPs of two batteries might form a short-circuit RBS structure, which is
 301 not allowed. To address this issue, a greedy algorithm incorporates as many SPs as possible while
 302 satisfying the reconstruction requirements.

303 The algorithm (see ~~pseudo-code~~ ~~the pseudocode~~ in Algorithm 1) is illustrated in Fig. 3 and is
 304 summarized as follows: First, the SPs are obtained by using Eqs. (13) and (14) in conjunction with
 305 the Dijkstra search. Next, the matrix \mathbf{A} is calculated using Eq. (1), and the initial N_{set} is set to N_b .
 306 The algorithm uses a dichotomy method to iteratively check until convergence different combinations
 307 of c_b batteries from N_b and updates N_{set} . For each combination, the algorithm constructs an effective
 308 solution if possible, and calculates the currents I_o and \mathbf{I}_b ~~by~~ using Eqs. (7) and (8). If the maximum
 309 current \mathbf{I}_b is less than or equal to I_m , η is calculated ~~by~~ using Eq. (10), and the maximum η is
 310 updated accordingly. Finally, the algorithm outputs the maximum η once N_{set} converges.

311 3 Case Study

312 3.1 Structures ~~and details~~

313 Currently, ~~there are~~ two types of RBS structures ~~have been proposed by Visairo et al.~~ ~~in the existing~~
 314 ~~literature — those of Visairo and Kumar~~ [11] and Lawson ~~et al.~~ [17], both of which have seen real
 315 use. The primary goal of Visairo ~~and Kumar~~'s structure (Fig. 4b) is to dynamically adjust the RBS
 316 output power. However, the isolation of unhealthy batteries is not sufficiently addressed in their
 317 work. Lawson ~~et al.~~ designed the RBS structure shown in Fig. 4a to isolate batteries. Although
 318 this structure easily isolates batteries, it cannot dynamically adjust the output current of the RBS.
 319 Based on the ~~structures~~ ~~structure~~ of Visairo and Kumar ~~and that of~~ Lawson, this paper proposes the
 320 structure shown in Fig. 4c. By integrating the Visairo ~~and Kumar~~ RBS structure into the Lawson
 321 RBS structure, the proposed structure not only has the flexibility to switch the batteries between
 322 series, parallel, and mixed series-parallel modes, ~~but also allows the isolation of highly degraded~~
 323 batteries from the RBS. ~~These four-battery RBS structures are investigated in~~
 324 ~~In~~ the case study, ~~including the scenarios with random isolated batteries.~~

325 3.2 Result

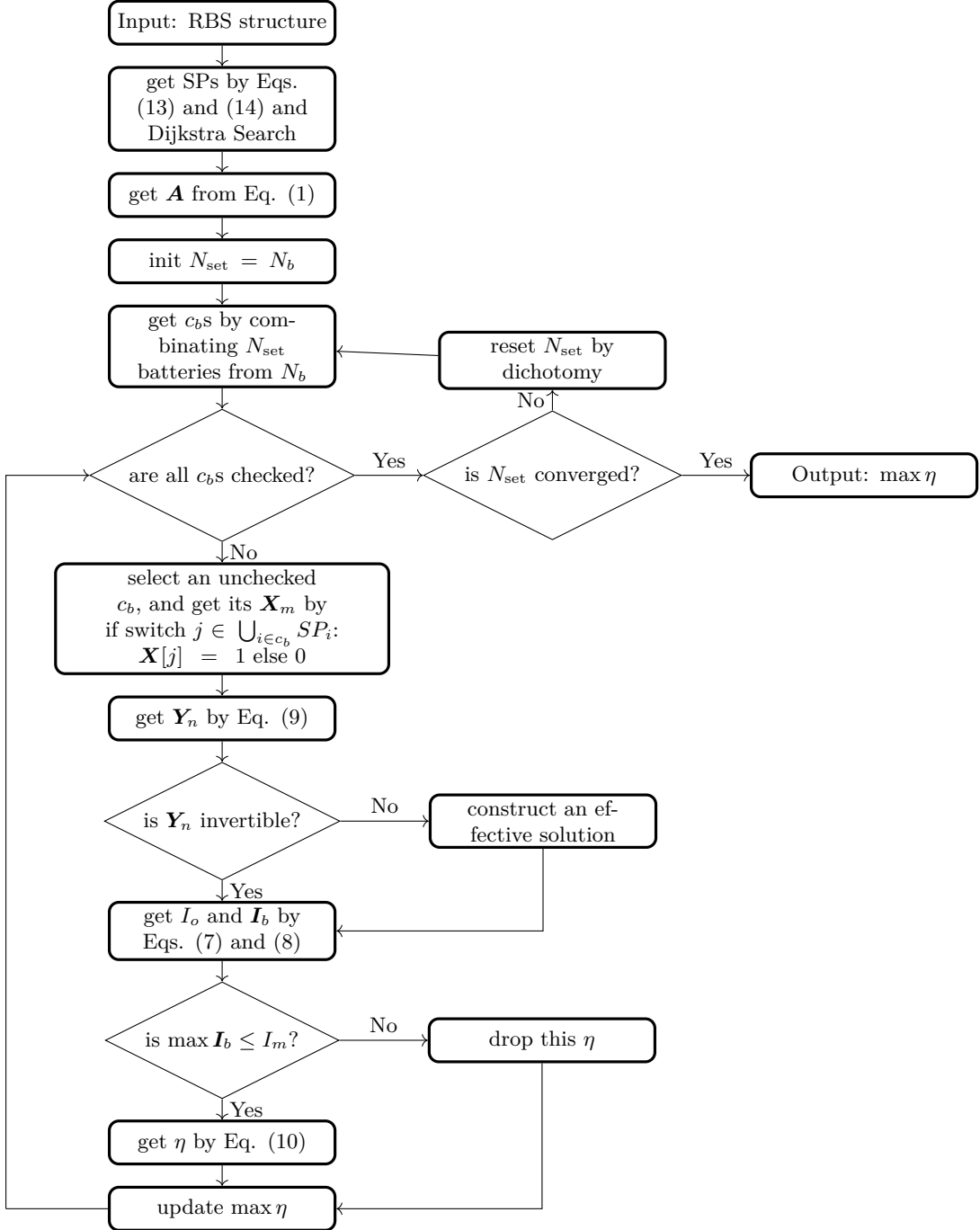


Figure 3: The computational flowchart of the MAC for a given RBS.

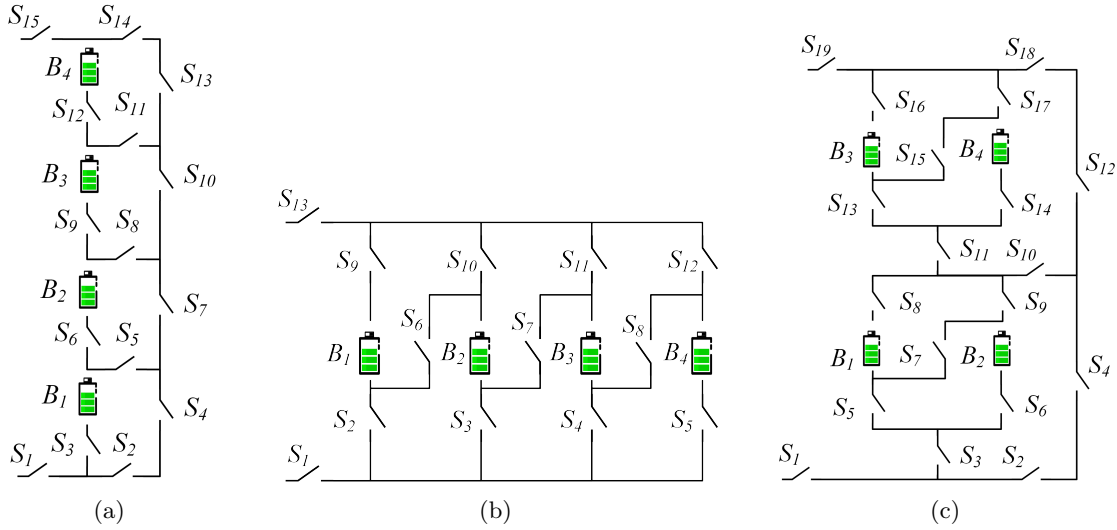


Figure 4: The four-battery RBS structures proposed by (a) Lawson [17], (b) Visairo and Kumar [11], and (c) this paper.

326 As shown the following RBS systems are investigated and compared: (a) three different structures
327 (Figs. 4a–4c) with the same four batteries; (b) the same structure as in Fig. 4c, the new RBS
328 structure consists of four batteries with two/four/six batteries; and (c) the four-battery structure in
329 Fig. 4c with random isolated batteries. The greedy algorithm proposed in this work is also compared
330 with the brute-force algorithm, SA, and 19 switches. Figure ?? shows the corresponding directed
331 graph, which is composed of 18 nodes and 43 edges. Batteries B_1, B_2, B_3 , and B_4 are denoted by
332 green directed edges in the graph, and the 19 switches are represented by gray directed edges with
333 bidirectional arrows. The external electrical load is treated as a directed edge from the cathode of
334 the RBS (i.e., node 18) to the anode (i.e., node GA to validate its effectiveness and efficiency. In
335 order to adapt the two heuristic algorithms to the system's structure and scale, the number of state
336 neighbors of SA and the population size of GA are both set to $N_b \cdot N_s$, which increases with the
337 number of batteries and switches in the system. The parameters of the other algorithms are shown
338 in Tab. 1.

Table 1: The SA and GA algorithm parameters.

Algorithm/parameter	Value
SA/initial temperature	100
SA/final temperature	1), as indicated by the blue directed edge in the graph.
SA/cooling rate	0.95
GA/total generations	100
GA/crossover probability	0.8
GA/mutation probability	0.02

339 **3.2 Result**

340 **3.2.1 The shortest path**

341 Using Eq. (13) and the Dijkstra algorithm, the SPs of the four batteries in the RBS ~~structure of~~
 342 ~~Fig. 4c are highlighted in red in Figs. ?? and ??.~~ Finally, the calculated structures of Figs. 4a, 4b,
 343 and 4c are calculated and highlighted with different colors in Figs. 5a, 5b, and 5c, respectively.

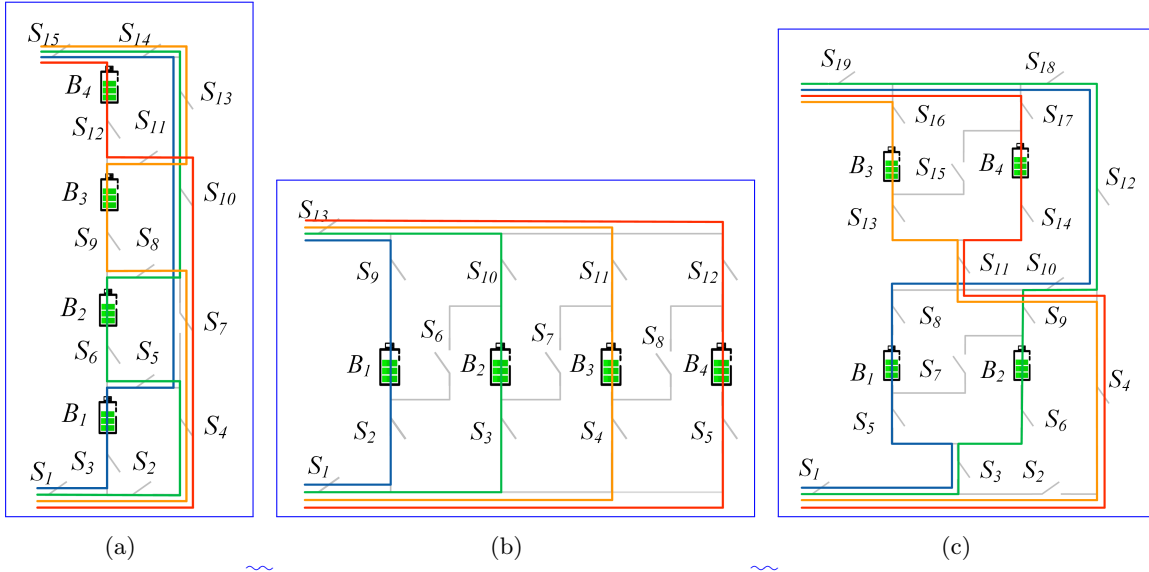


Figure 5: The SPs of the four batteries in the RBS structures of (a) Fig. 4a, (b) Fig. 4b, and (c) Fig. 4c.

344 **3.2.2 Three structures with four batteries**

345 After obtaining the SPs, the MACs of the ~~structure in Fig. 4e are listed in Tab. 4 and shown in~~
 346 ~~Fig. ??, as obtained by the greedy algorithm 1.~~ Tab. 4 three RBS structures with four batteries are
 347 ~~calculated using the proposed greedy algorithm, and the results are shown in Tabs. 2, 3, and 4, each~~
 348 ~~of which contains the states of the switches, the output current I_o , the battery current I_b , and the~~
 349 ~~ratio η of the RBS structure with all batteries in good health when the RBS when the system~~
 350 ~~output reaches the MAC. Fig. ?? presents the corresponding circuit, with the red highlight indicating that~~
 351 ~~the current is flowing through the respective branches.~~

352 ————— For the RBS structure in Fig. 4c, (a) its directed graph and the SPs
 353 (highlighted in red) of battery (b) B_1 , (c) B_2 , (d) B_3 , and (e) B_4 . (f) Circuit of RBS with its output
 354 reaching the MAC.

355 Calculated MAC for four-battery RBS structure in Fig. 4c. Structure Figure 4c with four
 356 batteries and 19 switches Switch on $S_1, S_3, S_5, S_6, S_8, S_9, S_{10}, S_{12}, S_{18}, S_{19}$ $I_o = 2u_b/(2R_o + r_b)$ $I_b = [u_b/(2R_o + r_b), u_b/(2R_o + r_b)]$,
 357 $\max \eta = 2$

358 Similarly, the results of the MAC calculation for the structures ~~The corresponding switch-control~~
 359 ~~schemes are shown as blue-highlighted electric currents in Figs. 4a and 4b are listed in Tabs. 2 and~~

360 [36a](#), [6b](#), and [6c](#), respectively.

361 To verify and compare the results from the proposed greedy algorithm, we also used a—the brute-
 362 force algorithm that which iterates through all possible switch states, and the heuristic algorithms
 363 (SA and GA) to calculate the MAC MACs of the same three RBSs. The final results of the brute-force
 364 algorithm are the same as the results shown in Tabs. 4–3. The method uses the greedy algorithm
 365 to calculate 11, 11, and 1 reconfigured structures for the RBS structure in Figs. 4c, 4a, and 4b,
 366 respectively. For the same RBS, the method those of the greedy algorithm and are shown in Tabs. 2,
 367 3, and 4. However, the brute-force algorithm counts all possible switch states, which equates to 2^{19} ,
 368 2^{15} , and 2^{13} , and 2^9 structures, respectively. The temporal evolutions of the objective values of the
 369 two heuristic algorithms during the iteration process are shown in Figs. 7a, 7b, and 7c, respectively,
 370 and compared with the proposed greedy algorithm. Compared with the SA and GA, the proposed
 371 greedy algorithm identifies the correct results within fewer iteration steps.

Table 2: [The calculated MAC Calculating result](#) of the four-battery RBS structure in Fig. 4a.

Structure	Figure 4a with 4-four batteries and 15 switches
Switch ON	$S_1, S_3, S_5, S_7, S_{10}, S_{13}, S_{14}, S_{15}$
I_o	$u_b/(R_o + r_b)$
I_b	$[u_b/(R_o + r_b), 0, 0, 0]$
$\max \eta$	1

Table 3: [The calculated MAC Calculating result](#) of the four-battery RBS structure in Fig. 4b.

Structure	Figure 4b with 4-four batteries and 13 switches
Switch ON	$S_1, S_2, S_3, S_4, S_5, S_9, S_{10}, S_{11}, S_{12}, S_{13}$
I_o	$4u_b/(4R_o + r_b)$
I_b	$[u_b/(4R_o + r_b), u_b/(4R_o + r_b), u_b/(4R_o + r_b), u_b/(4R_o + r_b)]$
$\max \eta$	4

372 Furthermore, the RBS with isolated batteries is taken into consideration and calculated. The
 373 MAC calculation

Table 4: [The calculated MAC of the four-battery RBS structure in Fig. 4c.](#)

Structure	Figure 4c with four batteries and 19 switches
Switch ON	$S_1, S_3, S_5, S_6, S_8, S_9, S_{10}, S_{12}, S_{18}, S_{19}$
I_o	$2u_b/(2R_o + r_b)$
I_b	$[u_b/(2R_o + r_b), u_b/(2R_o + r_b), 0, 0]$
$\max \eta$	2

373

3.2.3 Structures with different numbers of batteries

374 We next examine the RBS configurations depicted in Fig. 4c, which consist of two, four, and six
 375 batteries. The results for the three structures under study, with varying numbers of isolated batteries,

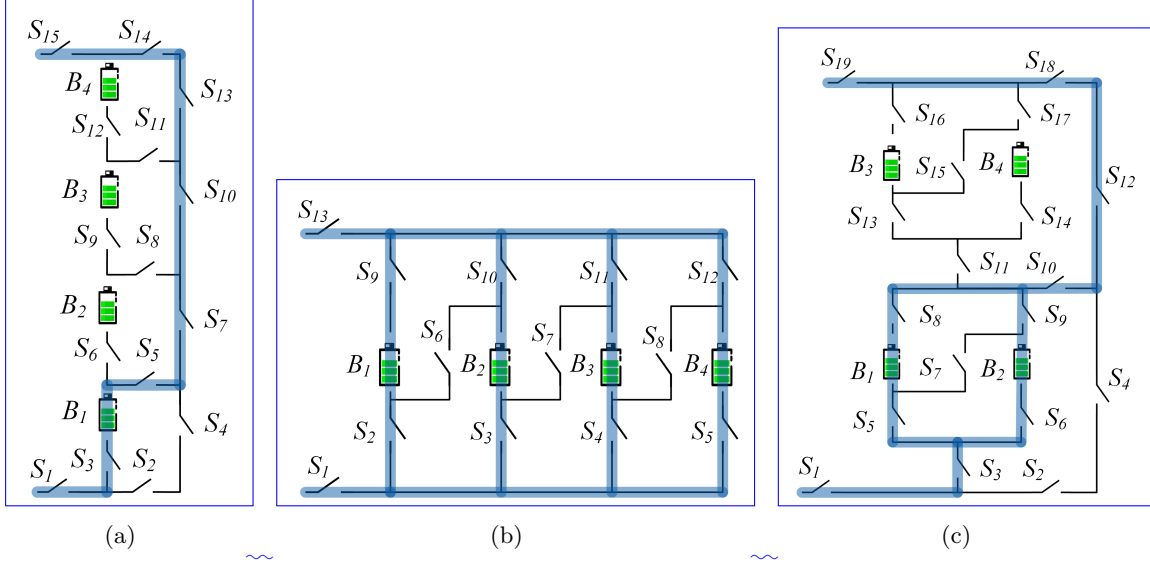


Figure 6: The RBS switch-control schemes with the output reaching the MAC.

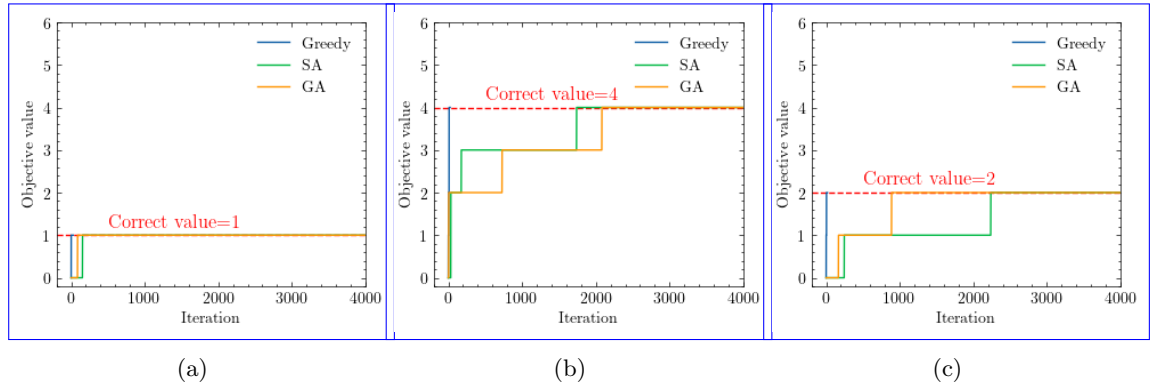


Figure 7: The temporal evolution of the objective values during the iteration process of calculating the RBS structures in (a) Fig. 4a, (b) Fig. 4b, and (c) Fig. 4c

377 four-battery configuration are presented in Tab. ???. Figs. 10a–10d illustrate the corresponding 4
 378 and Figs. 6c and 7c. The structures and final switch-control schemes for the new structure proposed
 379 in this paper under different conditions of isolated batteries two-battery and six-battery systems are
 380 illustrated in Figs. 8a and 8b, respectively. Furthermore, the temporal evolutions of the objective
 381 values throughout the iteration process are shown in Figs. 9a and 9b, respectively. The proposed
 382 greedy algorithm still converges the fastest and achieves the correct MAC. The SA algorithm fails
 383 to obtain the correct MAC within the given number of iteration steps in the case of the six-battery
 384 RBS structure.

Variation of MAC with the number of isolated batteries for different RBS structures, including the structure proposed by Lawson et al., Visairo et al., and the structure proposed in this paper. This

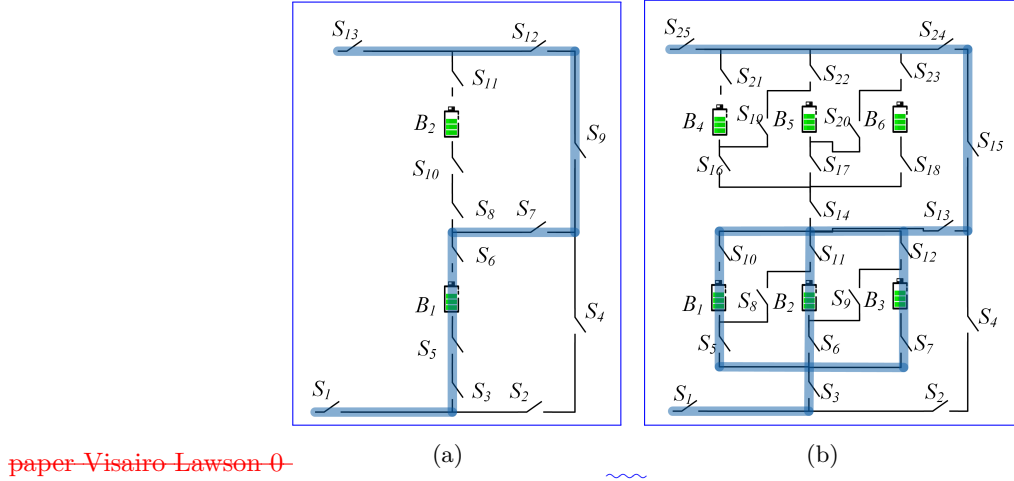


Figure 8: The (a) two-battery and (b) six-battery RBS switch-control schemes with the output reaching the MAC.

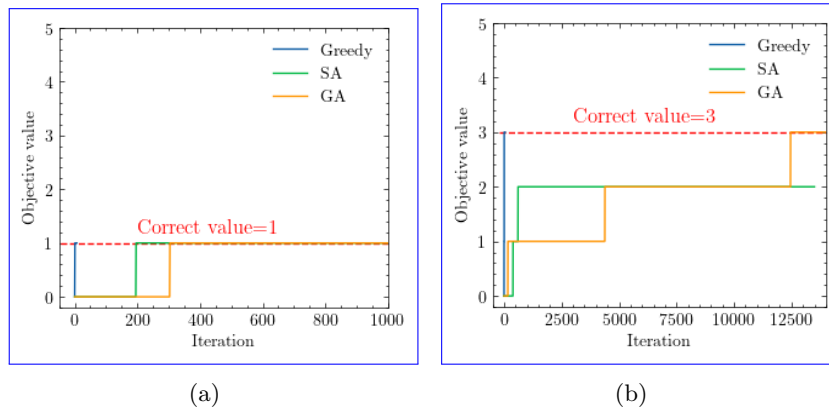


Figure 9: The temporal variation of the objective values during the iteration process of calculating the RBS structures in (a) Fig. 8a and (b) Fig. 8b.

385 **3.2.4 Random isolated batteries**

386 To assess the effectiveness of the proposed algorithm in the case of unhealthy batteries, the RBS with
 387 random isolated batteries is also taken into account and computed. In the case of the four-battery
 388 RBS structure depicted in Fig. 4c, there are four possible scenarios for isolated batteries: (a) a single
 389 unhealthy battery, (b) two unhealthy batteries located in different substructures, (c) two unhealthy
 390 batteries located in the same substructure, and (d) three unhealthy batteries. The resulting MAC
 391 (η) values for these four scenarios are 24-1-1, 23-, 12-2^a or -, and 1^b-2-1-3-1-1-1-, respectively.
 392 Furthermore, the corresponding switch-control schemes for the four scenarios are illustrated in Figs
 393 10a–10d.

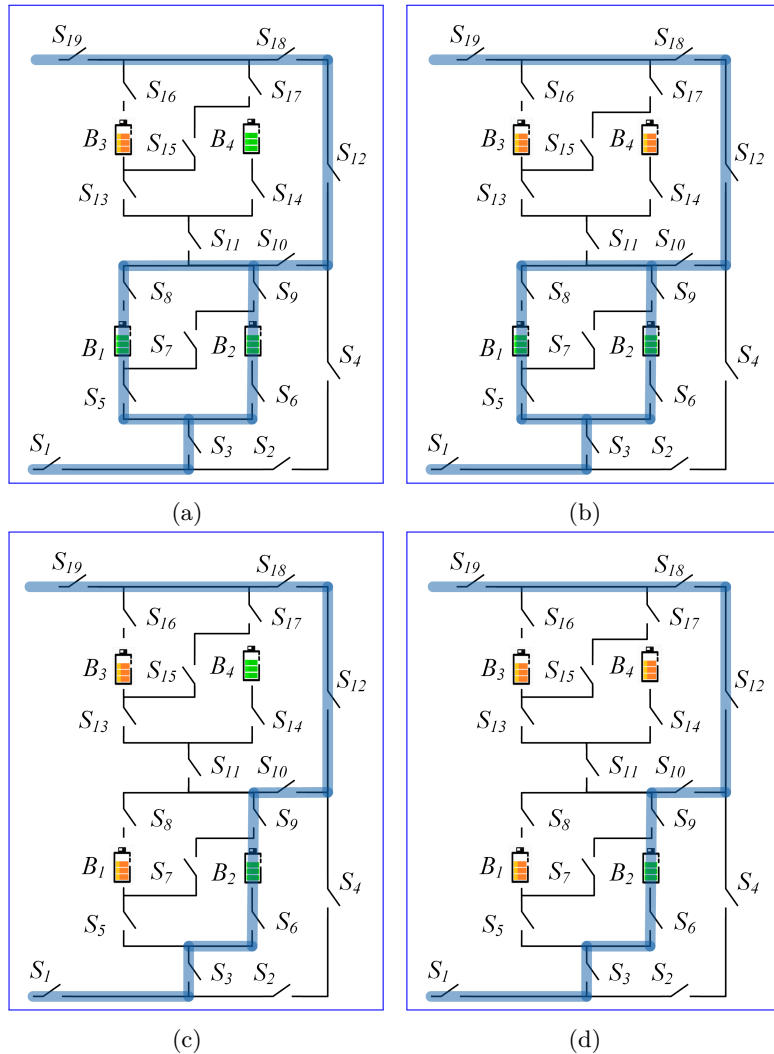


Figure 10: **Circuit**—The circuit states of MACs when isolating (a) one, (b) two (**best-case** in different substructures), (c) two (**worst-case** in the same substructure), and (d) three batteries for the structure in Fig. 4c.

394 **3.3 Discussion**

395 Consider first the results

396 **3.3.1 Result validation**

397 The correctness of the outcomes provided by the proposed greedy algorithm will now be discussed
398 from two perspectives: circuit analysis and validation against the brute-force algorithm. The result
399 of the four-battery RBS structure shown in Fig. ?? and listed in Tab. 4c is determined as an
400 example. When B_1 and B_2 or B_3 and B_4 are connected in parallel, the RBS outputs produces
401 the maximum current, which is $\eta = 2$ (i.e., twice the current output of a single battery in the
402 RBS). Adding more batteries to the main circuit only forms creates a series structure and does
403 not improve the MAC. Therefore, the state of the switches given switch-control scheme provided in
404 Tab. 4 maximizes the RBS output current. The brute-force method, which go through examines all
405 possible switch states, also gives the same result. yields the same η . This indicates that the proposed
406 greedy algorithm successfully identifies the MAC among all the potential reconfigured structures.

407 The literature contains no report on an algorithm for calculating the MAC of an RBS. The

408 **3.3.2 Pros and cons analysis**

409 The proposed greedy algorithm possesses a significant advantage in terms of its effectiveness and
410 efficiency. In this paper, it is compared with the brute-force algorithm, which goes through SA, and
411 GA. While the brute-force algorithm ensures the correctness of the results by exploring all possible
412 switch states, is the most straightforward way to determine the MAC and is used as a benchmark for
413 the it comes at a high computational cost. The SA and GA are commonly used heuristic algorithms
414 for addressing NP-hard problems. They selectively generate solutions for the switching states to
415 maximize the objective value η . However, neither of these two algorithms can determine whether
416 the current η represents the final MAC or if there are better solutions. Moreover, as depicted in
417 Figs. 7a–7c and Figs. 9a–9b, the SA and GA algorithms require more iterations to converge to the
418 final solution than the proposed greedy algorithm.

419 To further elaborate on the efficiency of our algorithm, we analyze the time complexity of both the
420 brute-force algorithm and the greedy algorithm. If an RBS has N_b batteries and N_s switches and the
421 corresponding directed graph has N nodes, 2^{N_s} iterations are required to traverse all reconfigured
422 possible structures. Calculating each reconfigured structure using Eqs. (7)–(10) requires matrix
423 inversion and matrix multiplication, which has results in a time complexity of $O(N^3 + 2N^2N_b +$
424 $N^2N_s + NN_b^2)$. Therefore, the time complexity of the brute-force algorithm is $O((N^3 + 2N^2N_b +$
425 $N^2N_s + NN_b^2)2^{N_s})$. The greedy algorithm proposed in this paper requires that the SP be found for
426 each battery, which requires N_b iterations. Each SP can be obtained by through several applications
427 of Dijkstra's algorithms. Therefore, the total time complexity for calculating all SPs is $O(N_b(N_b +$
428 $2N_s)\log_{10} N)$. According to Appendix 1, the RBS can reconfigure $C_{N_b}^{N_{set}}$ structures by selecting
429 N_{set} batteries from N_b batteries, which gives $\sum_{N_{set}=1}^{N_b} C_{N_b}^{N_{set}}/N_b \approx 2^{N_b}N_b^{-1}$ on average. Thus, with
430 the bisection method, the time complexity of the greedy algorithm is $O((N^3 + 2N^2N_b + N^2N_s +$
431 $NN_b^2)2^{N_b}N_b^{-1}\log_{10} N_b + N_b(N_b + 2N_s)\log_{10} N)$. Based on currently proposed RBS structures For

432 the existing RBS structures in the literature [39, 40, 41, 42, 43, 44], the number N_b of batteries, N_s
 433 of switches, and N of nodes of batteries N_b , the number of switches N_s , and the number of nodes N
 434 are quantitatively related as follows: $N_s \approx (3-5)N_b$, $N \approx N_s$. After simplifying, the time complexity
 435 of the method with the greedy algorithm is $O(2^{N_b} N_s^2 \log_{10} N_b)$, while it is $O(2^{N_s} N_s^3)$ for that of the
 436 method with brute-force algorithm the brute-force algorithm is $O(2^{N_s} N_s^3)$. Therefore, as the RBS
 437 grows, especially in terms of the number of switches, the greedy algorithm gains an advantage over
 438 the brute-force algorithm. This is confirmed by the number of structures required to determine the
 439 MAC in the previous section. Compared with the brute-force algorithm, the method based on the
 440 greedy algorithm is 3 000 to 48 000 times more efficient, which is theoretically $N_s 2^{N_s - N_b} \log_{10} N_b$
 441 times according to the above time-complexity analysis. This benefits from two key points is the result
 442 of two key factors:

- 443 (1) The SPs guide the RBS to reconfigure reasonable structures rather than blindly going through
 444 all possible structures. This reduces the complexity from 2^{N_s} to 2^{N_b} , which is the main reason
 445 for the improvement in efficiency.
- 446 (2) The bisection method further accelerates this process, reducing the complexity from 2^{N_b} to
 447 $2^{N_b} N_B^{-1} \log_{10} N_b$.

448 However, the greedy algorithm proposed in this paper still contains

449 Furthermore, this approach can handle RBSs with arbitrary structures, which is another significant
 450 advantage. It can even do this when they have different battery variations or even random isolated
 451 batteries. Theoretically, each RBS structure can be transformed into a unique directed graph model
 452 using the methodology described in Section II, and the MAC can subsequently be calculated using
 453 the proposed greedy algorithm. This finding is supported by the findings in the previous subsection.

454 However, the suggested greedy algorithm still includes exponential terms in the its time com-
 455 plexity, which means it may not be able to handle extremely large RBS structures having large
 456 N_b , indicating that it struggles to perform at scale. Additionally, all batteries are assumed to be
 457 identical for the sake of simplification in the derivation. However, in reality, there may exist a small
 458 balancing current that could introduce a minor bias in the MAC due to variations in the open-circuit
 459 voltage u_b and the internal resistance r_b . Nevertheless, the proposed greedy algorithm remains a
 460 viable choice for RBS design and optimization in the early stage, and the issue of balancing current
 461 bias can be addressed by considering the inconsistency between batteries and replacing the internal
 462 resistance with impedance when constructing the directed graph model.

464 3.3.3 Application scenarios

465 Note that η is used as the objective function instead of I_o in solving for the MAC. This choice makes
 466 the resulting MAC more reasonable and applicable to practical scenarios. As shown in Tab. 4, I_o
 467 and \mathbf{I}_b are functions of R_o , u_b , and r_b . However, when I_o is used as the objective function, even for
 468 the same RBS structure, the MAC solution and corresponding switch states could change due to
 469 different external electrical appliances. This would increase increases the difficulty and uncertainty

470 of involved in designing the RBS structure. To eliminate this problem, the ratio $\eta = I_o / \max I_b$
 471 $\eta = I_o / \max(I_b)$ is adopted as the objective function in our research. Recall that η reflects only the
 472 structure's ability to output current, rather than the actual current outputting output by the battery
 473 system. Assuming that the MAC of the batteries in the RBS is I_m , the maximum output current
 474 of the RBS structure can be calculated as ηI_m by determining the value of η for the structure.

475 The method proposed in this paper facilitates the design of RBSs in the following ways: ~~Most~~
 476 ~~currently proposed~~. Most of the existing RBS structures [39, 40, 41, 42, 43, 44] have simple
 477 topological characteristics, so calculating the their MACs is relatively straightforward, ~~or~~ even
 478 intuitive. However, these simple structures do not always fully satisfy the requirements of complex
 479 applications, such as dynamically adapting the circuit to variable and random operating conditions
 480 or actively equalizing differences between batteries in the RBS. Moreover, isolating the batteries
 481 disrupts the original regularity and symmetry of the topology, which complicates the otherwise
 482 simple structure, and the maximum output current of the system becomes more challenging to
 483 obtain. In contrast, the proposed method calculates the MAC of arbitrary RBS structures, notably
 484 the most notably complex and flexible RBS structures.

485 To illustrate this point, the MACs of three RBS structures mentioned above the RBS structure in
 486 Fig. 4c are calculated after isolating one or more of the batteries, as shown in Tab. ?? Specifically,
 487 for the structure presented in Fig. 4e, the corresponding circuit states for the MACs when isolating
 488 one to three batteries are depicted in Figs. 10a–10d. This structure has two cases in which two When
 489 a single battery is isolated, the RBS is still capable of outputting the maximum current, denoted
 490 as $\eta = 2$. When two batteries are isolated, there are two scenarios: one is to isolate isolating two
 491 batteries within the same substructure (Fig. 10b), in which case resulting in $\eta = 2$; the other is to
 492 isolate isolating one battery in each of the two substructures (Fig. 10c), in which case resulting in
 493 $\eta = 1$. The results in Figs. 10a–10d show that the proposed method provides reasonable outcomes
 494 for isolating any number of batteries in any position. Furthermore, the output current for the three
 495 RBSs with isolated batteries is also shown in Tab. ?? For the structure proposed by Lawson et
 496 al., the MAC is independent of the number of isolated batteries. However, for Visairo's structure,
 497 the MAC decreases upon increasing the number of isolated batteries. Nevertheless, the MAC of
 498 the structure proposed in this work falls between the MACs of these two structures. This result
 499 indicates that the structure proposed in this paper has a larger MAC than Lawson's for the same
 500 number of batteries and has a wider range of regulation of the output current If three batteries are
 501 isolated, the RBS can only output the current of a single battery, which is $\eta = 1$. Therefore, the
 502 battery management system can adjust the output current and control the RBS to reconfigure the
 503 corresponding structure based on the isolated batteries.

504 4 Conclusion

505 This paper proposes a pervasive has proposed a reliable and automated method to efficiently compute
 506 the MAC of an RBS. The method is implemented by using a greedy algorithm combined with
 507 an improved directed graph model. Not only does the method provides provide the same global
 508 MAC calculation results as the brute force brute-force method, but it also improves the calculation

efficiency by 3 000 to 48 000 times for three RBS structures in the case study demonstrates superior computational efficiency to both the brute-force algorithm and the heuristic algorithms (SA and GA). Theoretically, for an RBS with N_s switches and N_b batteries, the efficiency of the proposed method is $N_s 2^{N_s - N_b} \log_{10} N_b$ times that of the brute-force method, which is mainly because of using . This is primarily due to the utilization of the batteries' SPs to guide guiding the RBS to reconfigure reasonable structures rather than blindly going through all possible structures. The main Another advantage of this method is its ability capability to calculate the MAC-MACs of RBSs with arbitrary structures and varying batteries. Even in scenarios with random isolated batteries, the proposed method remains effective. This method helps to fully tap the current output potential can facilitate the full utilization of the RBS's current output potential, guide the RBS structure design and optimization in the design stage of the RBS structure, and assist in evaluating the current overload risk of the system risk of current overload in practical applications.

5 Appendix

Acknowledgments

Author Contributions

B. Xu conceived the main idea, formulated the overarching research goals and aims, designed the algorithm, and reviewed and revised the manuscript. G. Hua developed and analyzed the model, implemented the code and supporting algorithms, and wrote the initial draft. C. Qian provided critical review, commentary, and revisions. Q. Xia contributed to shaping the research, analysis, and manuscript. B. Sun conducted the research and investigation process. Y. Ren secured the funding and supervised the project. Z. Wang verified the results and provided necessary resources.

Funding

This work was supported by the National Natural Science Foundation of China (NSFC, No.52075028).

Conflicts of Interest

The authors declare that there is no conflict of interest regarding the publication of this article.

Data Availability

This work does not require any data to be declared or publicly disclosed.

Algorithm 1: Get Obtain the ~~max~~ maximum available currents current (MAC) of a certain given RBS

Data: Directed graph model $G(V, E)$ of the RBS
Result: $\max \eta$

```

1 for  $i \in E_b$  do
2    $P_i \leftarrow \{path|starts at v_1 and ends at v_n\};$ 
3    $SP_i \leftarrow p_i$  which has the minimum  $\omega(p_i)$  among all  $p_i \in P_i$ .
4 end
5 get  $\mathbf{A}$  by Eq. 1;
6 while not yet determined  $\max \eta$  do
7 end
8  $N_{set} \leftarrow$  number of selected SPs calculated by dichotomy;
9  $C_b \leftarrow$  set of all combinations of  $N_{set}$  batteries from  $N_b$ ;
10 for  $c_b \in C_b$  do
11    $\mathbf{x}_s \leftarrow$  list of all switches' states:  $x_s[j] = 1$  if  $j \in \bigcup_{i \in c_b} SP_i$  else 0;
12    $\mathbf{X} \leftarrow diag[1, 1, \dots, 1, \mathbf{x}_s];$ 
13   get  $\mathbf{Y}_n$  by Eq. 9;
14   if  $\mathbf{Y}_n$  is invertible then
15     | pass
16   else
17     | construct an effective solution
18   end
19   get  $I_o$  by Eq. 7;
20   get  $\mathbf{I}_b$  by Eq. 8;
21   if  $\max(\mathbf{I}_b) \leq I_m$  then
22     |  $\eta \leftarrow I_o / \max(\mathbf{I}_b);$ 
23   else
24     | break
25   end
26 end

```

537 References

- 538 [1] Yuqing Yang, Stephen Bremner, Chris Menictas, and Merlinde Kay. Battery energy storage
539 system size determination in renewable energy systems: A review. *Renewable and Sustainable*
540 *Energy Reviews*, 91:109–125, August 2018.
- 541 [2] Luanna Maria Silva de Siqueira and Wei Peng. Control strategy to smooth wind power output
542 using battery energy storage system: A review. *Journal of Energy Storage*, 35:102252, March
543 2021.
- 544 [3] Eugene Schwanbeck and Penni Dalton. International Space Station Lithium-ion Batteries for
545 Primary Electric Power System. In *2019 European Space Power Conference (ESPC)*, pages 1–1.
546 IEEE, September 2019.
- 547 [4] Lihua Zhang. Development and Prospect of Chinese Lunar Relay Communication Satellite.
548 *Space: Science & Technology*, 2021, January 2021.
- 549 [5] Jaephil Cho, Sookkyung Jeong, and Youngsik Kim. Commercial and research battery technologies
550 for electrical energy storage applications. *Progress in Energy and Combustion Science*,
551 48:84–101, June 2015.
- 552 [6] Naixing Yang, Xiongwen Zhang, BinBin Shang, and Guojun Li. Unbalanced discharging and
553 aging due to temperature differences among the cells in a lithium-ion battery pack with parallel
554 combination. *Journal of Power Sources*, 306:733–741, February 2016.
- 555 [7] Fei Feng, Xiaosong Hu, Lin Hu, Fengling Hu, Yang Li, and Lei Zhang. Propagation mechanisms
556 and diagnosis of parameter inconsistency within Li-Ion battery packs. *Renewable and*
557 *Sustainable Energy Reviews*, 112:102–113, September 2019.
- 558 [8] J. A. Jeevarajan and C. Winchester. Battery Safety Qualifications for Human Ratings. *Interface*
559 *magazine*, 21(2):51–55, January 2012.
- 560 [9] Daniel Vázquez Pombo. A Hybrid Power System for a Permanent Colony on Mars. *Space:*
561 *Science & Technology*, 2021, January 2021.
- 562 [10] Weiji Han, Torsten Wik, Anton Kersten, Guangzhong Dong, and Changfu Zou. Next-
563 Generation Battery Management Systems: Dynamic Reconfiguration. *IEEE Industrial Elec-*
564 *tronics Magazine*, 14(4):20–31, December 2020.
- 565 [11] H. Visairo and P. Kumar. A reconfigurable battery pack for improving power conversion effi-
566 ciency in portable devices. In *2008 7th International Caribbean Conference on Devices, Circuits*
567 *and Systems*, pages 1–6. IEEE, April 2008.
- 568 [12] Song Ci, Ni Lin, and Dalei Wu. Reconfigurable battery techniques and systems: A survey.
569 *IEEE Access*, 4:1175–1189, 2016.

- 570 [13] Nejmeddine Bouchhima, Matthias Gossen, Sascha Schulte, and Kai Peter Birke. Lifetime of
571 self-reconfigurable batteries compared with conventional batteries. *Journal of Energy Storage*,
572 15:400–407, 2018.
- 573 [14] Song Ci, Jiucui Zhang, Hamid Sharif, and Mahmoud Alahmad. A novel design of adaptive
574 reconfigurable multicell battery for power-aware embedded networked sensing systems.
575 In *IEEE GLOBECOM 2007-IEEE Global Telecommunications Conference*, pages 1043–1047.
576 IEEE, 2007.
- 577 [15] Jan Engelhardt, Tatiana Gabderakhmanova, Gunnar Rohde, and Mattia Marinelli. Reconfigurable
578 stationary battery with adaptive cell switching for electric vehicle fast-charging. In *2020
579 55th International Universities Power Engineering Conference (UPEC)*, pages 1–6, 2020.
- 580 [16] Jan Engelhardt, Jan Martin Zepter, Tatiana Gabderakhmanova, Gunnar Rohde, and Mattia
581 Marinelli. Double-string battery system with reconfigurable cell topology operated as a fast
582 charging station for electric vehicles. *Energies*, 14(9):2414, 2021.
- 583 [17] Barrie Lawson. A Software Configurable Battery. *EVS26 International Battery, Hybrid and
584 Fuel Cell Electric Vehicle Symposium*, pages 252–263, 2012.
- 585 [18] Liang He, Linghe Kong, Siyu Lin, Shaodong Ying, Yu Gu, Tian He, and Cong Liu.
586 Reconfiguration-assisted charging in large-scale lithium-ion battery systems. In *2014
587 ACM/IEEE International Conference on Cyber-Physical Systems (ICCPs)*, pages 60–71. IEEE,
588 2014.
- 589 [19] Hahnsang Kim and Kang G Shin. On dynamic reconfiguration of a large-scale battery system.
590 In *2009 15th IEEE Real-Time and Embedded Technology and Applications Symposium*, pages
591 87–96. IEEE, 2009.
- 592 [20] Weiji Han and Anton Kersten. Analysis and Estimation of the Maximum Circulating Current
593 during the Parallel Operation of Reconfigurable Battery Systems. In *2020 IEEE Transportation
594 Electrification Conference & Expo (ITEC)*, pages 229–234. IEEE, June 2020.
- 595 [21] Jan Engelhardt, Jan Martin Zepter, Tatiana Gabderakhmanova, Gunnar Rohde, and Mattia
596 Marinelli. Double-String Battery System with Reconfigurable Cell Topology Operated as a Fast
597 Charging Station for Electric Vehicles. *Energies*, 14(9):2414, 2021.
- 598 [22] Weiji Han, Anton Kersten, Changfu Zou, Torsten Wik, Xiaoliang Huang, and Guangzhong
599 Dong. Analysis and estimation of the maximum switch current during battery system recon-
600 figuration. *IEEE Transactions on Industrial Electronics*, 69(6):5931–5941, 2021.
- 601 [23] Lidiya Komsytska, Tobias Buchberger, Simon Diehl, Moritz Ehrensberger, Christian Hanzl,
602 Christoph Hartmann, Markus Hözle, Jan Kleiner, Meinert Lewerenz, Bernhard Liebhart,
603 Michael Schmid, Dominik Schneider, Sascha Speer, Julia Stöttner, Christoph Terbrack, Michael
604 Hinterberger, and Christian Endisch. Critical Review of Intelligent Battery Systems: Chal-
605 lenges, Implementation, and Potential for Electric Vehicles. *Energies*, 14(18):5989, 2021.

- 606 [24] Luis D. Couto and Michel Kinnaert. Partition-based Unscented Kalman Filter for Recon-
 607 figurable Battery Pack State Estimation using an Electrochemical Model. In *2018 Annual*
 608 *American Control Conference (ACC)*, pages 3122–3128. IEEE, June 2018.
- 609 [25] Anton Kersten, Manuel Kuder, Weiji Han, Torbjorn Thiringer, Anton Lesnicar, Thomas Weyh,
 610 and Richard Eckerle. Online and On-Board Battery Impedance Estimation of Battery Cells,
 611 Modules or Packs in a Reconfigurable Battery System or Multilevel Inverter. In *IECON 2020*
 612 *The 46th Annual Conference of the IEEE Industrial Electronics Society*, pages 1884–1891. IEEE,
 613 October 2020.
- 614 [26] Michael Schmid, Emanuel Gebauer, Christian Hanzl, and Christian Endisch. Active Model-
 615 Based Fault Diagnosis in Reconfigurable Battery Systems. *IEEE Transactions on Power Elec-*
 616 *tronics*, 36(3):2584–2597, March 2021.
- 617 [27] Jan Kacel, Jingyang Fang, Tomas Kacel, Nima Tashakor, and Stefan Goetz. Design and
 618 Analysis of Modular Multilevel Reconfigurable Battery Converters for Variable Bus Voltage
 619 Powertrains. *IEEE Transactions on Power Electronics*, 38(1):130–142, January 2023.
- 620 [28] Feng Yang, Fei Gao, Baochang Liu, and Song Ci. An Adaptive Control Framework for Dynam-
 621 ically Reconfigurable Battery Systems Based on Deep Reinforcement Learning. *IEEE Transac-*
 622 *tions on Industrial Electronics*, 69(12):12980–12987, December 2022.
- 623 [29] Weiji Han, Changfu Zou, Liang Zhang, Quan Ouyang, and Torsten Wik. Near-Fastest Battery
 624 Balancing by Cell/Module Reconfiguration. *IEEE Transactions on Smart Grid*, 10(6):6954–
 625 6964, November 2019.
- 626 [30] Xinghua Liu, Guoyi Chang, Jiaqiang Tian, Zhongbao Wei, Xu Zhang, and Peng Wang. Flexible
 627 path planning-based reconfiguration strategy for maximum capacity utilization of battery pack.
 628 *Journal of Energy Chemistry*, 86:362–372, November 2023.
- 629 [31] Si-Zhe Chen, Yule Wang, Guidong Zhang, Le Chang, and Yun Zhang. Sneak Circuit Theory
 630 Based Approach to Avoiding Short-Circuit Paths in Reconfigurable Battery Systems. *IEEE*
 631 *Transactions on Industrial Electronics*, 68(12):12353–12363, 2021.
- 632 [32] Kailong Liu, Zhongbao Wei, Chenghui Zhang, Yunlong Shang, Remus Teodorescu, and Qing-
 633 Long Han. Towards Long Lifetime Battery: AI-Based Manufacturing and Management. *IEEE/-*
 634 *CAA Journal of Automatica Sinica*, 9(7):1139–1165, July 2022.
- 635 [33] Morteza Mollajafari. An efficient lightweight algorithm for scheduling tasks onto dynamically
 636 reconfigurable hardware using graph-oriented simulated annealing. *Neural Computing and Ap-*
 637 *plications*, 35(24):18035–18057, August 2023.
- 638 [34] Liang He, Linghe Kong, Siyu Lin, Shaodong Ying, Yu Gu, Tian He, and Cong Liu.
 639 Reconfiguration-assisted charging in large-scale Lithium-ion battery systems. In *2014*
 640 *ACM/IEEE International Conference on Cyber-Physical Systems (ICCPs)*, pages 60–71. IEEE,
 641 April 2014.

- 642 [35] Zoltan Mark Pinter, Dimitrios Papageorgiou, Gunnar Rohde, Mattia Marinelli, and Chresten
 643 Traholt. Review of Control Algorithms for Reconfigurable Battery Systems with an Industrial
 644 Example. In *2021 56th International Universities Power Engineering Conference (UPEC)*,
 645 pages 1–6, August 2021.
- 646 [36] Liang He, Lipeng Gu, Linghe Kong, Yu Gu, Cong Liu, and Tian He. Exploring Adaptive
 647 Reconfiguration to Optimize Energy Efficiency in Large-Scale Battery Systems. In *2013 IEEE*
 648 *34th Real-Time Systems Symposium*, pages 118–127, December 2013.
- 649 [37] Hongwen He, Rui Xiong, Xiaowei Zhang, Fengchun Sun, and JinXin Fan. State-of-Charge
 650 Estimation of the Lithium-Ion Battery Using an Adaptive Extended Kalman Filter Based on
 651 an Improved Thevenin Model. *IEEE Transactions on Vehicular Technology*, 60(4):1461–1469,
 652 May 2011.
- 653 [38] S.M. Mousavi G. and M. Nikdel. Various battery models for various simulation studies and
 654 applications. *Renewable and Sustainable Energy Reviews*, 32:477–485, April 2014.
- 655 [39] Song Ci, Jiucai Zhang, Hamid Sharif, and Mahmoud Alahmad. A Novel Design of Adaptive
 656 Reconfigurable Multicell Battery for Power-Aware Embedded Networked Sensing Systems. In
 657 *IEEE GLOBECOM 2007-2007 IEEE Global Telecommunications Conference*, pages 1043–1047,
 658 November 2007.
- 659 [40] Mahmoud Alahmad, Herb Hess, Mohammad Mojarradi, William West, and Jay Whitacre. Bat-
 660 tery switch array system with application for JPL’s rechargeable micro-scale batteries. *Journal*
 661 *of Power Sources*, 177(2):566–578, March 2008.
- 662 [41] Hahnsang Kim and Kang G. Shin. Dependable, efficient, scalable architecture for management
 663 of large-scale batteries. In *Proceedings of the 1st ACM/IEEE International Conference on Cyber-*
 664 *Physical Systems, ICCPS ’10*, pages 178–187, New York, NY, USA, April 2010. Association for
 665 Computing Machinery.
- 666 [42] Younghyun Kim, Sangyoung Park, Yanzhi Wang, Qing Xie, Naehyuck Chang, Massimo Pon-
 667 cino, and Massoud Pedram. Balanced reconfiguration of storage banks in a hybrid electrical
 668 energy storage system. In *2011 IEEE/ACM International Conference on Computer-Aided De-*
 669 *sign (ICCAD)*, pages 624–631, November 2011.
- 670 [43] Taesic Kim, Wei Qiao, and Liyan Qu. A series-connected self-reconfigurable multicell battery
 671 capable of safe and effective charging/discharging and balancing operations. In *2012 Twenty-*
 672 *Seventh Annual IEEE Applied Power Electronics Conference and Exposition (APEC)*, pages
 673 2259–2264, February 2012.
- 674 [44] Liang He, Linghe Kong, Siyu Lin, Shaodong Ying, Yu Gu, Tian He, and Cong Liu.
 675 Reconfiguration-assisted charging in large-scale Lithium-ion battery systems. In *2014*
 676 *ACM/IEEE International Conference on Cyber-Physical Systems (ICCPs)*, pages 60–71, April
 677 2014.

¹ Determining Maximum Allowable Current of an RBS using a
² Directed Graph Model and Greedy Algorithm

³ Binghui Xu^{1†}, Guangbin Hua^{1†}, Cheng Qian^{1*}, Quan Xia^{1,2}, Bo Sun¹, Yi Ren¹, and
⁴ Zili Wang¹

⁵ ¹School of Reliability and Systems Engineering, Beihang University, Beijing, 100191,
⁶ China

⁷ ²School of Aeronautic Science and Engineering at Beihang University, Beijing, China

⁸ *Address correspondence to: cqian@buaa.edu.cn

⁹ [†]These authors contributed equally to this work.

10

Abstract

11

Reconfigurable battery systems provide a promising alternative to traditional battery systems due to their flexible and dynamically changeable topological structures that can be adapted to different battery charging and discharging strategies. A critical system parameter known as the maximum allowable current (MAC) is pivotal to RBS operation. This parameter is instrumental in maintaining the current of each individual battery within a safe range and serves as a guiding indicator for the system's reconfiguration, ensuring its safety and reliability. This paper proposes a method for calculating the MAC of an arbitrary RBS using a greedy algorithm in conjunction with a directed graph model of the RBS. Using the shortest path of the battery, the greedy algorithm transforms the exhaustion of the switch states in the brute-force algorithm or variable search without utilizing structures in the heuristic algorithms in the combination of the shortest paths. The directed graph model, based on an equivalent circuit, provides a specific method for calculating the MAC of a given structure. The proposed method is validated using two previously published RBS structures and an additional one with a more complex structure. The results are the same as those from the brute-force algorithm, but the proposed method significantly improves the computational efficiency, being theoretically $N_s 2^{N_s - N_b} \log_{10} N_b$ times faster than the brute-force algorithm for an RBS with N_b batteries and N_s switches. Another advantage of the proposed method is its ability to calculate the MAC of RBSs with arbitrary structures and variable batteries, even in scenarios with random isolated batteries.

29

1 Introduction

30

Battery energy storage systems (BESSs) are widely utilized in various applications [1], such as wind power plants [2] and space power systems [3, 4], for the purpose of storing and releasing high-quality

32 electrical energy [5]. Typically, a BESS consists of numerous batteries interconnected by series-
33 parallel circuitry to provide the required storage capacity. However, conventional BESSs, in which
34 the batteries are connected in a fixed topology, suffer from a significant weakness in their worst
35 batteries due to the so-called cascading effect. Furthermore, if the worst battery fails during operation, it
36 is highly likely to accelerate the degradation of the other batteries, resulting in reliability and safety
37 issues at the system level [6, 7, 8]. These challenges have become major technical obstacles in many
38 engineering projects that demand high reliability, such as the development of next-generation space
39 vehicles [9]. Reconfigurable battery systems (RBSs), which can dynamically switch between different
40 circuit topologies as needed, are expected to be able to address these issues [10]. In a typical RBS,
41 additional switches are introduced between the batteries to form a reconfigurable network, where the
42 circuit's topology can be altered by opening or closing the switches. By opening the switches adjacent
43 to the unhealthy batteries, they can be isolated from the system, ensuring that the system remains
44 in a reliable operational state [11]. Furthermore, an RBS can be reconfigured to adapt to different
45 charging and discharging strategies, thereby enhancing the system's efficiency and prolonging the
46 battery's lifespan [12]. These advantages make RBSs a promising alternative to traditional BESSs.

47 The early research on RBSs mainly focused on the topological design of their structures, incor-
48 porating different levels of flexibility and reconfigurability to meet application requirements. For
49 example, Ci et al. [13] proposed an RBS structure that dynamically adjusts the battery discharge
50 rate to fully exploit the available capacity of each battery. Jan et al. [14, 15] designed structures that
51 reconfigure circuits with variant batteries in series to accommodate the constantly changing voltage
52 requirements during electric vehicle charging. A structure proposed by Visairo and Kumar [16] alters
53 the system's output voltage based on the load conditions, thereby reducing power loss in the voltage
54 regulator during the power supply process and enhancing energy efficiency. Lawson [17] and He et
55 al. [18] also focused on enhancing energy efficiency, and proposed simplified structures that have
56 fewer switches than the design of Visairo and Kumar. Kim et al. [19] improved the ability of an RBS
57 structure to recover from battery failures by introducing multiple ports. These complex structures
58 between batteries and switches provide flexibility to RBSs but also pose challenges in hardware de-
59 sign. During the reconfiguration process, current deviation and fluctuation may occur. Specifically,
60 when the system switches from series to parallel connection, a circulating current between parallel
61 cells can be triggered due to a voltage imbalance [20]. Failure to fully consider this issue during the
62 design of RBSs can result in damage to the batteries, switches, and wires. For example, Engelhardt
63 et al. [21] applied an RBS to a fast-charging scenario with adaptive cell switching to balance cell
64 states while adhering to voltage requests. However, the switching of batteries leads to intolerable
65 current variations. To address this problem, Han et al. [22] derived an analytical expression for the
66 maximum switch current during battery system reconfiguration. This analytical expression aids in
67 the selection of switches and supports general hardware design.

68 Recently, increasing attention has been paid to the estimation and control of RBS system states,
69 and several approaches have been proposed to optimize the performance of these systems. State
70 estimation, which is an essential technology in traditional battery management systems, serves as
71 the foundation for system control and holds great potential in the context of RBSs [23]. Couto et al.
72 [24] introduced a partition-based unscented Kalman filter to estimate the state of a large-scale RBS,

73 utilizing an enhanced reduced-order electrochemical model. Kersten et al. [25] utilized the balancing
74 current of neighboring cells in parallel operation to determine the battery impedance, thereby
75 obtaining information about the state of health and power capability of the RBS. Schmid et al. [26]
76 further leveraged the reconfigurable nature of the system to actively diagnose faults, employing an
77 algorithm that changes the system structure to enhance the fault isolability. Another active research
78 area is the development of effective control strategies for RBSs to achieve optimal performance, in-
79 cluding improved stability [27] and efficiency [28]. Han et al. [29] proposed a near-fastest battery
80 balancing algorithm to minimize the time required for battery charge equalization. Liu et al. [30]
81 also proposed a scheme for maximizing capacity utilization based on a path planning algorithm,
82 aiming to enhance the battery consistency within the system. To break through the bottleneck
83 of the potential short-circuit paths increasing exponentially with the RBS scale, Chen et al. [31]
84 proposed a systematic approach based on sneak circuit theory. They conducted a comprehensive
85 analysis of all paths between the cathode and anode of each battery in the RBS, identifying paths
86 that consist only of switches as short-circuit paths for pre-checking before system reconfiguration.
87 Artificial intelligence has also appeared in RBS management [32]. The effectiveness of the deep
88 reinforcement learning method has been validated in real-world RBSs [28].

89 The maximum allowable current (MAC), which is defined as the maximum current allowed within
90 the constraints of a battery cell, is a crucial indicator of RBSs that need to be evaluated during the
91 design and control of the system. The MAC assists designers in assessing whether the RBS meets
92 output current requirements and contributes to the development of appropriate and safe strategies
93 for the battery management system. However, few studies have directly determined the MACs of
94 RBSs, primarily due to the complexity arising from reconfiguration. In the field of computer science,
95 there is a similar problem with scheduling tasks on dynamically reconfigurable hardware with limited
96 resources and task interdependencies. This problem is analogous to the determination of the MAC
97 and a corresponding solution has been proposed [33, 34]. However, dealing with the structural
98 characteristics and circuit equations of RBSs is challenging for this method. From the perspective
99 of RBS structure analysis, the MAC problem can be transformed into a problem of finding the
100 maximum output current among all possible reconfigurations of the RBS. However, this may be
101 an NP-hard problem [35]. Common methods such as brute-force algorithms, simulated annealing
102 (SA) algorithms, and genetic algorithms (GA) have the drawbacks of inefficiency, excessive time
103 consumption, and an inability to guarantee the globally optimal solution.

104 To solve this issue, this paper proposes an efficient method to evaluate the MACs of RBSs. In this
105 method, a greedy algorithm is designed to efficiently search the possible circuit topologies of RBSs.
106 This algorithm transforms the inefficient search for reconfigurations into a proactive combining of
107 the shortest paths of the batteries. Furthermore, an improved directed graph model is introduced to
108 analyze the current of the RBS, taking into account factors such as the voltage, internal resistance,
109 MAC of the battery, and external load. The main contributions of this study can be summarized as
110 follows:

- 111 • An efficient method is proposed to determine the MACs of RBSs with arbitrary structures,
112 including scenarios with isolated batteries.

- 113 • A greedy algorithm is applied to solve the MAC problem, the computational complexity of
114 which is greatly reduced compared with the brute-force algorithm.

115 • An improved directed graph model is introduced to provide a specific method for calculating
116 the MAC of a given structure.

117 The remainder of this paper is organized as follows: Section II presents the framework and
118 details of the proposed directed graph model and the greedy algorithm. Section III applies the
119 proposed method to determine the MACs of two published RBS structures and a new one with a
120 more complex structure. The calculation results, the computational complexity of the algorithm,
121 and scenarios such as battery random isolation are also discussed. Finally, the concluding remarks
122 are presented in Section IV.

123 2 Methodology

124 The central principle of the proposed method is to connect the batteries in an RBS in parallel to the
125 maximum possible extent, thereby maximizing the output current. To achieve this universally and
126 automatically, the overall process is divided into the four steps shown in Fig. 1. First, a directed
127 graph model is established for the subsequent computations. The model not only contains the
128 connected relationships between batteries and switches but also retains the performance parameters
129 of the batteries. Subsequently, based on the equivalent circuit, the MAC problem is transformed
130 into specific objective functions and constraints. The shortest paths (SPs, where additional batteries
131 and switches on the path are penalized for distance) of the batteries are then obtained using the
132 Dijkstra algorithm to connect the batteries in the RBS in parallel. Finally, a greedy algorithm is
133 used to organize the switches, allowing the batteries to connect via their SPs while satisfying the
134 constraints, resulting in the MAC of the RBS.

135 2.1 Directed graph model

136 He et al. [36] proposed an abstracted directed graph model for an RBS, where the nodes represent the
137 batteries, the edges represent the configuration flexibility, and the weight of each vertex corresponds
138 to the battery voltage (Fig. 2a). The model captures all potential system configurations and offers
139 a direct metric for configuration flexibility, but it does not specify the physical implementation
140 of the connectivity between batteries, meaning that one graph might correspond to multiple RBS
141 structures. We previously proposed a directed graph model that differs significantly from He et al.'s
142 model by using nodes to represent the connections between batteries and switches and directed edges
143 to represent batteries and switches (Fig. 2b), allowing for a one-to-one correspondence between an
144 RBS structure and its directed graph model. This model accurately and comprehensively represents
145 the RBS topological structure but cannot be used for quantitative MAC calculations because it
146 does not consider the voltage, internal resistance, or MAC of the battery. To address this issue, we
147 improve our previous model by adding electromotive force and resistance attributes on the edges
148 based on the corresponding equivalent circuits. The model also considers the external load as an

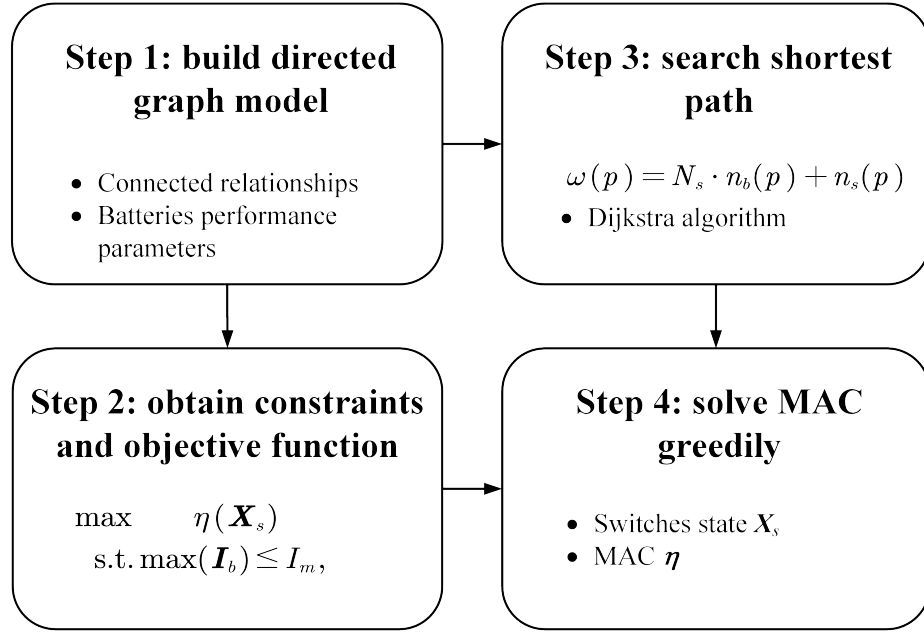


Figure 1: A diagram of the proposed method, which contains four main steps.

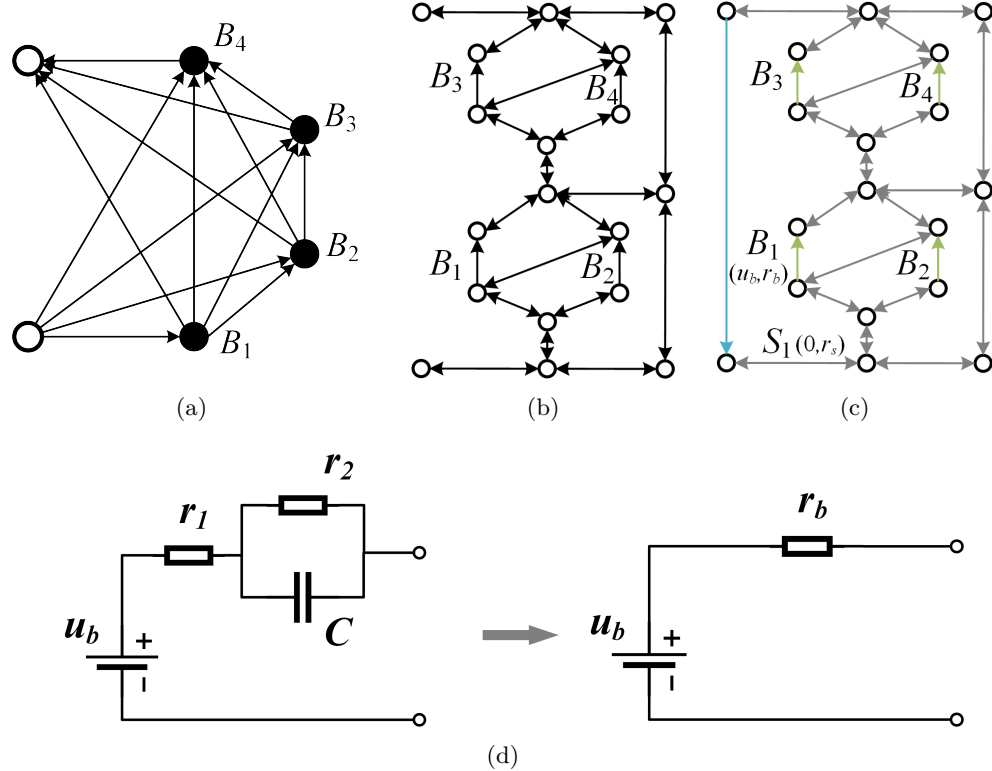


Figure 2: The directed graph models used in (a) the work of He et al. [36], (b) our previous work, and (c) the improved model in this paper. (d) The equivalent circuit of a battery in this method.

equivalent resistance and integrates it into the analysis, making it a complete circuit model for later circuit analysis. Fig. 2c shows the improved directed graph model used in this paper. The following provides a detailed explanation of the method used for equating components in RBSs and constructing the directed graph model.

To use circuit analysis methods to solve the MAC of the RBS, the components in the RBS are equated to ideal circuit elements. For instance, as shown in Fig. 2d, the battery in the RBS is represented as a black-box circuit consisting of two resistors r_1 and r_2 and a capacitor C , in what is known as the Thevenin model [37, 38]. With an emphasis on the stable output of the RBS, the capacitor in the Thevenin model can be considered as an open circuit without affecting the steady-state current. Therefore, battery B_i in the RBS can be simplified as a series connection between a constant voltage source u_i and a resistor r_i . Furthermore, the state of the switch S_j in the RBS is represented by a binary variable x_j , where 0 is ON and 1 is OFF. When the switch is closed, the circuit can be regarded as a resistor with a very small resistance r_j . Finally, the external load is considered as a resistor with resistance R_o .

For a given RBS structure, its directed graph model $G(V, E)$ is constructed as follows:

1. Nodes: The nodes in the directed graph correspond to the connection points of components in the actual RBS. Assuming there are a total of N nodes in the RBS, for the sake of convenience, the anode of the RBS is denoted as v_1 and the cathode as v_N .
2. Edges: The edges in the directed graph correspond to the batteries, switches, and external electrical loads in the actual RBS. Therefore, there are three types of directed edges. For battery B_i , its directed edge e_i is drawn from the cathode to the anode because the battery in operation only allows current to flow in one direction. For switch S_j , since it is allowed to work under bidirectional currents, it is represented by a pair of directed edges with two-way directions. For the external electrical load, because it is connected to the anode and cathode of the RBS, a directed edge from v_N to v_1 is used to represent it. In conclusion, for a given RBS structure with N_b batteries and N_s switches, the number of directed edges is $N_b + 2N_s + 1$, where 1 represents the external electrical load.
3. Attributes of edges: Each edge is assigned two attributes, a voltage difference and a resistance, based on the equivalent method mentioned above. The values for battery B_i , switch S_j , and the external loads correspond to (u_i, r_i) , $(0, r_j)$, and $(0, R_o)$, respectively.

2.2 Constraints and objective function

For a given RBS, determining the MAC involves maximizing the RBS output current while ensuring that all battery currents do not exceed the batteries' MAC. This subsection establishes the constraints and objective function used to determine the MAC through circuit analysis based on the directed graph model provided in the previous section.

First, the topology in the directed graph model is represented in the form of a matrix \mathbf{A} , which

185 is known as the incidence matrix and is defined as follows:

$$a_{kl} = \begin{cases} 1, & \text{edge } l \text{ leaves node } k, \\ -1, & \text{edge } l \text{ enters node } k, \\ 0, & \text{otherwise.} \end{cases} \quad (1)$$

186 For a directed graph consisting of N nodes and $N_b + 2N_s + 1$ directed edges, the incidence matrix \mathbf{A}
187 is an $N \times (N_b + 2N_s + 1)$ matrix. In this matrix, the rows and columns represent the nodes and edges
188 of the directed graph, respectively. By distinguishing the components in the RBS corresponding to
189 each column, \mathbf{A} can be rewritten as

$$\mathbf{A} = [\mathbf{A}_b \quad \mathbf{A}_s \quad \mathbf{A}_o], \quad (2)$$

190 where \mathbf{A}_b , \mathbf{A}_s , and \mathbf{A}_o are the submatrices corresponding to the batteries, switches, and external
191 electrical load, respectively. To reduce the computational complexity, the dimensions of matrix \mathbf{A} are
192 reduced. Since each directed edge has one node to leave and one to enter, the values in every column
193 of \mathbf{A} sum to zero. Therefore, removing the last row will not result in a loss of information. Conversely,
194 since each switch in the RBS is represented by a pair of directed edges with two-way directions, the
195 two columns corresponding to the switch are mutually opposite. Thus, for the submatrix \mathbf{A}_s , only
196 one column is retained for each pair of columns representing the same switch. As a result, \mathbf{A} can
197 be reduced to an $(N - 1) \times (N_b + N_s + 1)$ matrix, denoted $\tilde{\mathbf{A}}$, for further calculation of the current
198 and voltage. Similar to Eq. (2), $\tilde{\mathbf{A}}$ can be rewritten as

$$\tilde{\mathbf{A}} = [\tilde{\mathbf{A}}_b \quad \tilde{\mathbf{A}}_s \quad \tilde{\mathbf{A}}_o]. \quad (3)$$

199 After obtaining the incidence matrix, the currents of all batteries and output in the RBS are
200 determined by solving the circuit equations. According to Kirchhoff's laws, we have

$$\begin{cases} \tilde{\mathbf{A}}\mathbf{I} = \mathbf{0}, \\ \mathbf{U} = \tilde{\mathbf{A}}^T \mathbf{U}_n, \end{cases} \quad (4)$$

201 where \mathbf{I} and \mathbf{U} indicate the current and voltage difference arrays of the $N_b + N_s + 1$ edges, respectively,
202 and \mathbf{U}_n is the voltage array of the $N - 1$ nodes. These directed edges are treated as generalized
203 branches and expressed in matrix form as follows:

$$\mathbf{I} = \mathbf{Y}\mathbf{X}\mathbf{U} - \mathbf{Y}\mathbf{X}\mathbf{U}_s + \mathbf{I}_s, \quad (5)$$

204 where \mathbf{U}_s and \mathbf{I}_s denote the source voltage and source current of the generalized branches, respec-
205 tively. Because all batteries have been made equivalent to voltage sources rather than current sources
206 in the previous subsection, all elements of the array \mathbf{I}_s are zero, whereas the elements of the array
207 \mathbf{U}_s are equal to the first attribute of the corresponding edges in the directed graph. The matrix \mathbf{Y} in
208 Eq. (5) is the admittance matrix of the circuit and is defined as the inverse of the impedance matrix.

209 The elements on the diagonal of matrix \mathbf{Y} are equal to the reciprocal of the resistance, which is the
 210 second attribute of the corresponding edges in the directed graph. The off-diagonal elements of \mathbf{Y}
 211 are zero. \mathbf{X} is the state matrix that determines whether the RBS batteries and switches can pass
 212 current. It is defined as

$$\mathbf{X} = \text{diag}(\underbrace{1, 0, \dots, 1}_{N_b \text{ of } 0/1}, \underbrace{1, 0, \dots, 1}_{N_s \text{ of } 0/1}, 1) = \begin{bmatrix} \mathbf{X}_b & & \\ & \mathbf{X}_s & \\ & & 1 \end{bmatrix}, \quad (6)$$

213 where element x_i of matrix \mathbf{X}_b indicates whether battery B_i has been removed from the circuit, with
 214 $x_i = 1$ indicating removal and $x_i = 0$ indicating that battery B_i is still available to supply power.
 215 When all batteries are healthy and capable of providing current to the external load, \mathbf{X}_b is the
 216 identity matrix. The elements x_j of matrix \mathbf{X}_s determine whether switch S_j is closed, with $x_j = 1$
 217 indicating a closed switch and $x_j = 0$ indicating an open switch, consistently with the previous
 218 subsection.

219 Theoretically, the output current I_o and the currents of each battery \mathbf{I}_b in the RBS can be
 220 determined by solving Eqs. (4)–(6) under any given state \mathbf{X} . To further simplify the problem, it
 221 is assumed that all batteries have the same electromotive force and internal resistance, which are
 222 denoted u_b and r_b , respectively. This allows us to derive explicit expressions for I_o and \mathbf{I}_b . After
 223 derivation and simplification, the output current I_o and the currents of each battery \mathbf{I}_b are ultimately
 224 represented as in Eqs. (7) and (8), respectively:

$$I_o = \frac{1}{R_o r_b} \tilde{\mathbf{A}}_o^T \mathbf{Y}_n^{-1}(\mathbf{X}) \tilde{\mathbf{A}}_b \mathbf{U}_b, \quad (7)$$

$$\mathbf{I}_b = \frac{1}{r_b^2} [\tilde{\mathbf{A}}_b^T \mathbf{Y}_n^{-1}(\mathbf{X}) \tilde{\mathbf{A}}_b \mathbf{U}_b - r_b \mathbf{U}_b], \quad (8)$$

225 where \mathbf{U}_b is an $N_b \times 1$ array with all elements equal to u_b , and \mathbf{Y}_n is the equivalent admittance
 226 matrix of the circuit and is defined as

$$\mathbf{Y}_n(\mathbf{X}) = \frac{1}{R_o} \tilde{\mathbf{A}}_o \tilde{\mathbf{A}}_o^T + \frac{1}{r_b} \tilde{\mathbf{A}}_b \mathbf{X}_b \tilde{\mathbf{A}}_b^T + \frac{1}{r_s} \tilde{\mathbf{A}}_s \mathbf{X}_s \tilde{\mathbf{A}}_s^T. \quad (9)$$

228 To characterize the current output capacity of the RBS structure under different switching states,
 229 an indicator η is defined by the ratio of I_o to $\max(\mathbf{I}_b)$:

$$\eta = \frac{I_o}{\max(\mathbf{I}_b)}. \quad (10)$$

230 Finally, the problem of finding the MAC can be formulated as

$$\max \eta(\mathbf{X}_s) \quad (11)$$

$$\text{s.t. } \max(\mathbf{I}_b) \leq I_m, \quad (12)$$

231 where I_m is the MAC of the battery.

232 However, it remains computationally difficult to solve Eq. (11) because of \mathbf{Y}_n^{-1} . Firstly, the in-
 233 troduction of nonlinear terms through \mathbf{Y}_n^{-1} renders many methods in linear optimization unsuitable
 234 for this problem. Secondly, the rank of \mathbf{Y}_n is proportional to the number of batteries and switches,
 235 which can be very large for a large RBS, leading to a significant computational burden. As a result,
 236 intelligent algorithms that rely on evolution by iteration may face efficiency problems when dealing
 237 with a large RBS. To address this issue, the problem should be considered from the perspective
 238 of guiding the RBS to reconstruct as many parallel structures as possible. Consequently, a greedy
 239 algorithm based on the shortest path is proposed. The detailed implementation of this algorithm is
 240 presented in the following two subsections.

241 2.3 Shortest path

242 The path p used in this method is defined as the complete route that passes through one battery
 243 (or a consecutive series of batteries) and closed switches, connecting the anode v_1 to the cathode v_N
 244 of the RBS. By applying a penalty to the series-connected batteries on the path, where additional
 245 batteries imply a greater distance, the algorithm encourages the RBS to form parallel structures to
 246 the maximum extent possible. In addition, to reduce the number of switches controlled during the
 247 reconstruction process, a penalty is also applied to the total number of switches on the path while
 248 ensuring the minimum number of batteries. Therefore, the distance ω of path p is

$$\omega(p) = N_s n_b(p) + n_s(p), \quad (13)$$

249 where N_s is the total number of switches in the system, and $n_b(p)$ and $n_s(p)$ are the number of
 250 batteries and switches along path p , respectively. Moreover, the shortest path SP_i is defined as the
 251 path with the minimum ω for battery B_i :

$$SP_i = \arg \min_{p \in P_i} \omega(p), \quad (14)$$

252 where P_i is the set of all paths from v_1 to v_N that pass through directed edge i .

253 SP_i can be solved using the Dijkstra algorithm. The Dijkstra algorithm is a graph-search method
 254 that finds the shortest path between two given nodes in a weighted graph, efficiently solving the
 255 single-source shortest-path problem. Denoting the cathode and anode of battery B_i as v_i^- and v_i^+
 256 respectively, path p of battery B_i can be divided into three segments: $v_1 \rightarrow v_i^-$, $v_i^+ \rightarrow v_N$, and
 257 $v_i^- \rightarrow v_i^+$. $v_i^- \rightarrow v_i^+$ is the directed edge corresponding to battery B_i . With the Dijkstra algorithm,
 258 the shortest paths for $v_1 \rightarrow v_i^-$ and $v_i^+ \rightarrow v_N$ can be calculated under the weights given in Eq. (13)
 259 and denoted $SP(v_i^- \rightarrow v_i^+)$ and $SP(v_i^+ \rightarrow v_N)$, respectively. Finally, SP_i for battery B_i is formed
 260 by the complete path, which consists of $SP(v_1 \rightarrow v_i^-)$, $v_i^- \rightarrow v_i^+$, and $SP(v_i^+ \rightarrow v_N)$.

261 2.4 Greedy algorithm

262 From the perspective of series vs. parallel connections, integrating more batteries into the circuit
 263 through their shortest paths (SPs) results in more batteries connected in parallel, thereby increasing

264 the total output current of the RBS. However, conflicts may arise between the SPs of different
265 batteries. For instance, the SPs of two batteries might form a short-circuit RBS structure, which is
266 not allowed. To address this issue, a greedy algorithm incorporates as many SPs as possible while
267 satisfying the reconstruction requirements.

268 The algorithm (see the pseudocode in Algorithm 1) is illustrated in Fig. 3 and is summarized as
269 follows: First, the SPs are obtained by using Eqs. (13) and (14) in conjunction with the Dijkstra
270 search. Next, the matrix \mathbf{A} is calculated using Eq. (1), and the initial N_{set} is set to N_b . The
271 algorithm uses a dichotomy method to iteratively check until convergence different combinations of
272 c_b batteries from N_b and updates N_{set} . For each combination, the algorithm constructs an effective
273 solution if possible, and calculates the currents I_o and \mathbf{I}_b using Eqs. (7) and (8). If the maximum
274 current \mathbf{I}_b is less than or equal to I_m , η is calculated using Eq. (10), and the maximum η is updated
275 accordingly. Finally, the algorithm outputs the maximum η once N_{set} converges.

276 3 Case Study

277 3.1 Structures and details

278 Currently, there are two types of RBS structures in the existing literature — those of Visairo and
279 Kumar [16] and Lawson [17], both of which have seen real use. The primary goal of Visairo and
280 Kumar’s structure (Fig. 4b) is to dynamically adjust the RBS output power. However, the isolation
281 of unhealthy batteries is not sufficiently addressed in their work. Lawson designed the RBS structure
282 shown in Fig. 4a to isolate batteries. Although this structure easily isolates batteries, it cannot
283 dynamically adjust the output current of the RBS. Based on the structure of Visairo and Kumar
284 and that of Lawson, this paper proposes the structure shown in Fig. 4c. By integrating the Visairo
285 and Kumar RBS structure into the Lawson RBS structure, the proposed structure not only has the
286 flexibility to switch the batteries between series, parallel, and mixed series-parallel modes, but also
287 allows the isolation of highly degraded batteries from the RBS.

288 In the case study, the following RBS systems are investigated and compared: (a) three different
289 structures (Figs. 4a–4c) with the same four batteries; (b) the same structure as in Fig. 4c with
290 two/four/six batteries; and (c) the four-battery structure in Fig. 4c with random isolated batteries.
291 The greedy algorithm proposed in this work is also compared with the brute-force algorithm, SA,
292 and GA to validate its effectiveness and efficiency. In order to adapt the two heuristic algorithms to
293 the system’s structure and scale, the number of state neighbors of SA and the population size of GA
294 are both set to $N_b \cdot N_s$, which increases with the number of batteries and switches in the system.
295 The parameters of the other algorithms are shown in Tab. 1.

296 3.2 Result

297 3.2.1 The shortest path

298 Using Eq. (13) and the Dijkstra algorithm, the SPs of the four batteries in the RBS structures of
299 Figs. 4a, 4b, and 4c are calculated and highlighted with different colors in Figs. 5a, 5b, and 5c,

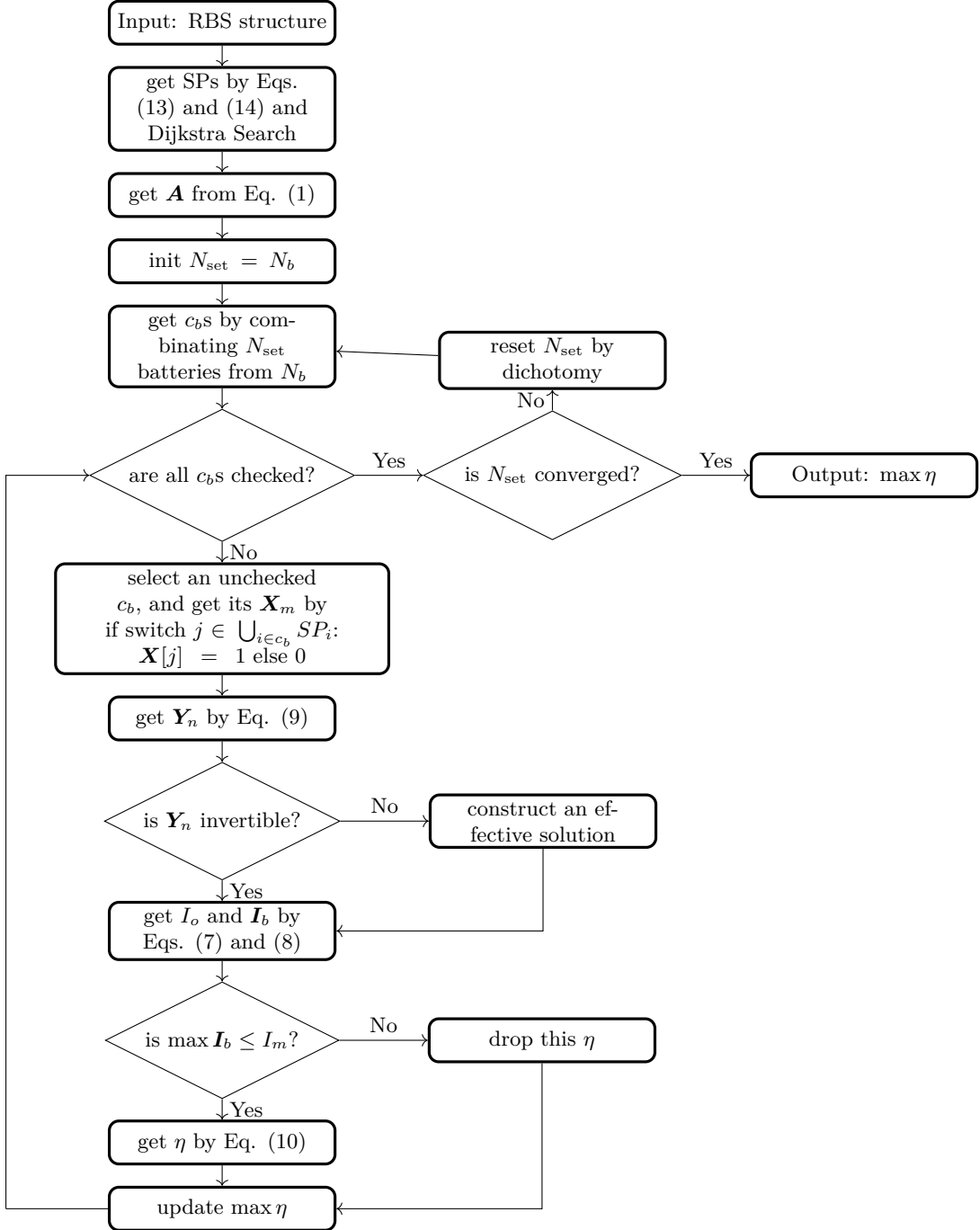


Figure 3: The computational flowchart of the MAC for a given RBS.

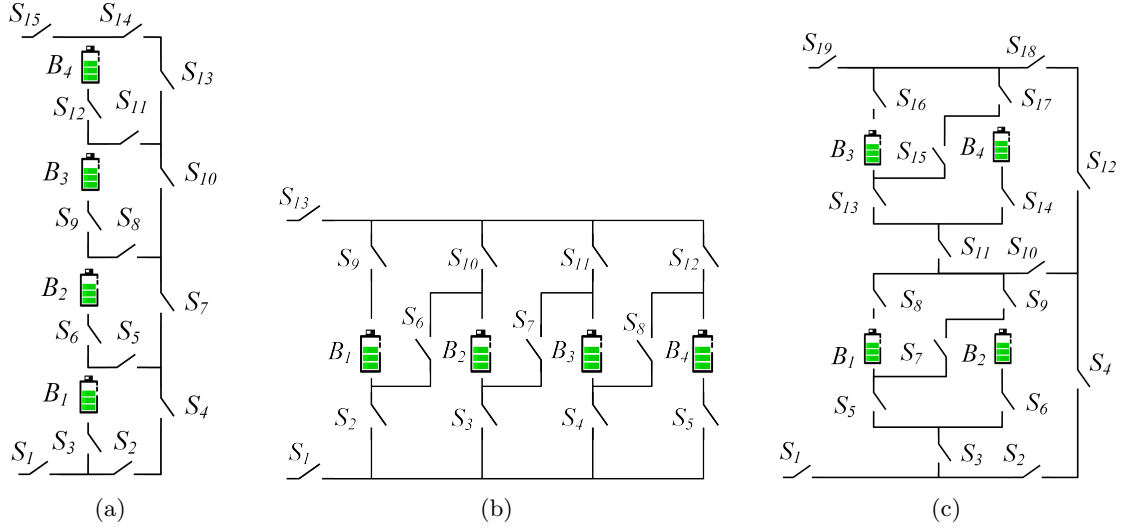


Figure 4: The four-battery RBS structures proposed by (a) Lawson [17], (b) Visairo and Kumar [16], and (c) this paper.

Table 1: The SA and GA algorithm parameters.

Algorithm/parameter	Value
SA/initial temperature	100
SA/final temperature	1
SA/cooling rate	0.95
GA/total generations	100
GA/crossover probability	0.8
GA/mutation probability	0.02

300 respectively.

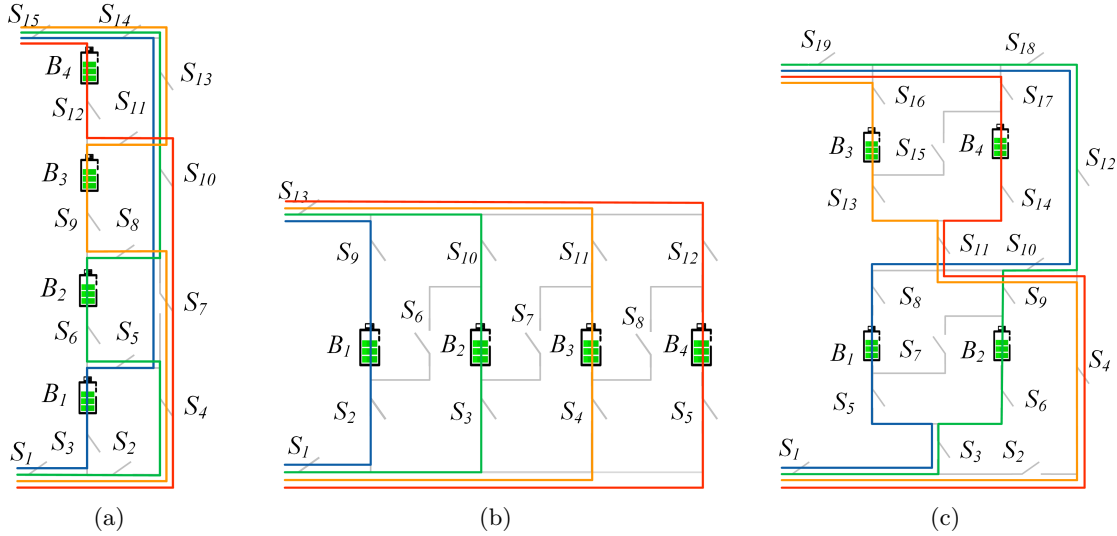


Figure 5: The SPs of the four batteries in the RBS structures of (a) Fig. 4a, (b) Fig. 4b, and (c) Fig. 4c.

3.2.2 Three structures with four batteries

302 After obtaining the SPs, the MACs of the three RBS structures with four batteries are calculated
 303 using the proposed greedy algorithm, and the results are shown in Tabs. 2, 3, and 4, each of which
 304 contains the states of the switches, the output current I_o , the battery current \mathbf{I}_b , and the ratio η
 305 when the system output reaches the MAC. The corresponding switch-control schemes are shown
 306 as blue-highlighted electric currents in Figs. 6a, 6b, and 6c, respectively. To verify and compare
 307 the proposed greedy algorithm, we also used the brute-force algorithm, which iterates through all
 308 possible switch states, and the heuristic algorithms (SA and GA) to calculate the MACs of the same
 309 RBSs. The final results of the brute-force algorithm are the same as those of the greedy algorithm
 310 and are shown in Tabs. 2, 3, and 4. However, the brute-force algorithm counts all possible switch
 311 states, which equates to 2^{15} , 2^{13} , and 2^{19} structures, respectively. The temporal evolutions of the
 312 objective values of the two heuristic algorithms during the iteration process are shown in Figs. 7a,
 313 7b, and 7c, respectively, and compared with the proposed greedy algorithm. Compared with the SA
 314 and GA, the proposed greedy algorithm identifies the correct results within fewer iteration steps.

Table 2: The calculated MAC of the four-battery RBS structure in Fig. 4a.

Structure	Figure 4a with four batteries and 15 switches
Switch ON	$S_1, S_3, S_5, S_7, S_{10}, S_{13}, S_{14}, S_{15}$
I_o	$u_b/(R_o + r_b)$
\mathbf{I}_b	$[u_b/(R_o + r_b), 0, 0, 0]$
$\max \eta$	1

Table 3: The calculated MAC of the four-battery RBS structure in Fig. 4b.

Structure	Figure 4b with four batteries and 13 switches
Switch ON	$S_1, S_2, S_3, S_4, S_5, S_9, S_{10}, S_{11}, S_{12}, S_{13}$
I_o	$4u_b/(4R_o + r_b)$
I_b	$[u_b/(4R_o + r_b), u_b/(4R_o + r_b), u_b/(4R_o + r_b), u_b/(4R_o + r_b)]$
$\max \eta$	4

Table 4: The calculated MAC of the four-battery RBS structure in Fig. 4c.

Structure	Figure 4c with four batteries and 19 switches
Switch ON	$S_1, S_3, S_5, S_6, S_8, S_9, S_{10}, S_{12}, S_{18}, S_{19}$
I_o	$2u_b/(2R_o + r_b)$
I_b	$[u_b/(2R_o + r_b), u_b/(2R_o + r_b), 0, 0]$
$\max \eta$	2

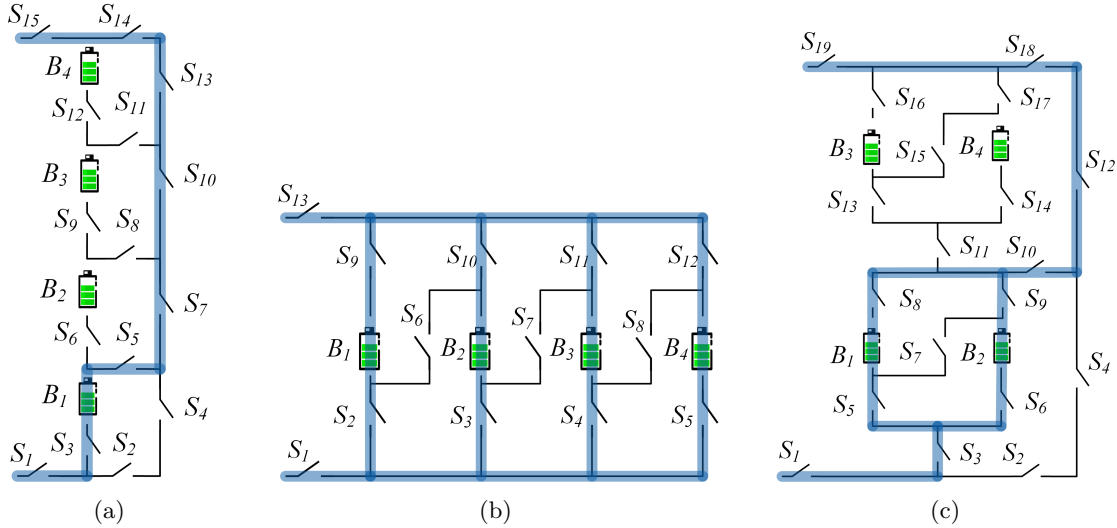


Figure 6: The RBS switch-control schemes with the output reaching the MAC.

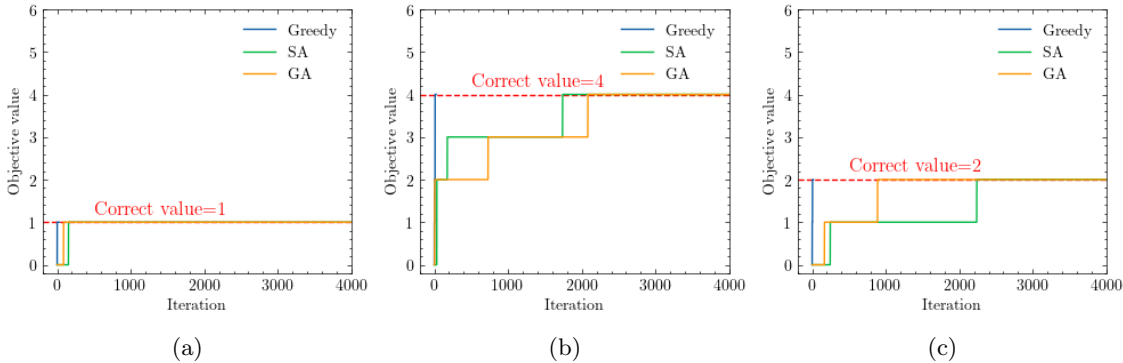


Figure 7: The temporal evolution of the objective values during the iteration process of calculating the RBS structures in (a) Fig. 4a, (b) Fig. 4b, and (c) Fig. 4c

315 **3.2.3 Structures with different numbers of batteries**

316 We next examine the RBS configurations depicted in Fig. 4c, which consist of two, four, and six
 317 batteries. The results for the four-battery configuration are presented in Tab. 4 and Figs. 6c and
 318 7c. The structures and final switch-control schemes for the two-battery and six-battery systems are
 319 illustrated in Figs. 8a and 8b, respectively. Furthermore, the temporal evolutions of the objective
 320 values throughout the iteration process are shown in Figs. 9a and 9b, respectively. The proposed
 321 greedy algorithm still converges the fastest and achieves the correct MAC. The SA algorithm fails
 322 to obtain the correct MAC within the given number of iteration steps in the case of the six-battery
 323 RBS structure.

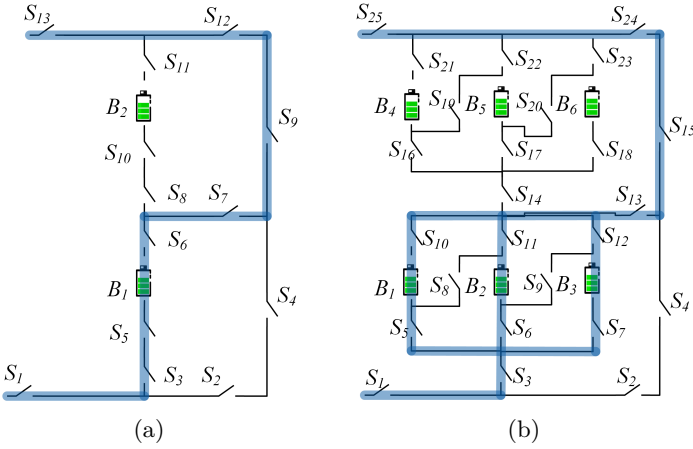


Figure 8: The (a) two-battery and (b) six-battery RBS switch-control schemes with the output reaching the MAC.

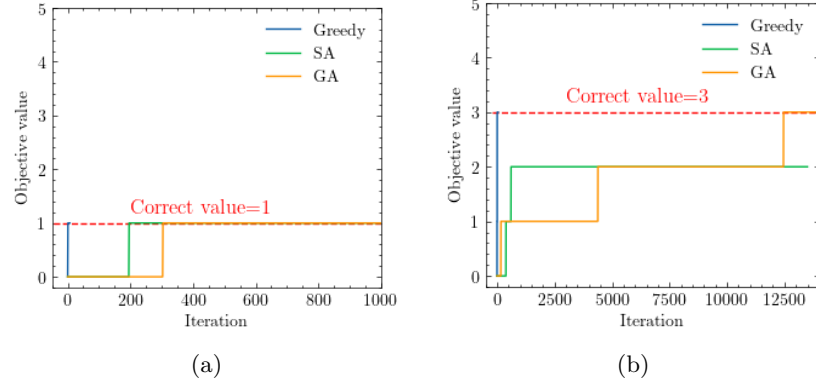


Figure 9: The temporal variation of the objective values during the iteration process of calculating the RBS structures in (a) Fig. 8a and (b) Fig. 8b.

324 **3.2.4 Random isolated batteries**

325 To assess the effectiveness of the proposed algorithm in the case of unhealthy batteries, the RBS with
 326 random isolated batteries is also taken into account and computed. In the case of the four-battery
 327 RBS structure depicted in Fig. 4c, there are four possible scenarios for isolated batteries: (a) a single
 328 unhealthy battery, (b) two unhealthy batteries located in different substructures, (c) two unhealthy
 329 batteries located in the same substructure, and (d) three unhealthy batteries. The resulting MAC
 330 (η) values for these four scenarios are 2, 2, 1, and 1, respectively. Furthermore, the corresponding
 331 switch-control schemes for the four scenarios are illustrated in Figs 10a–10d.

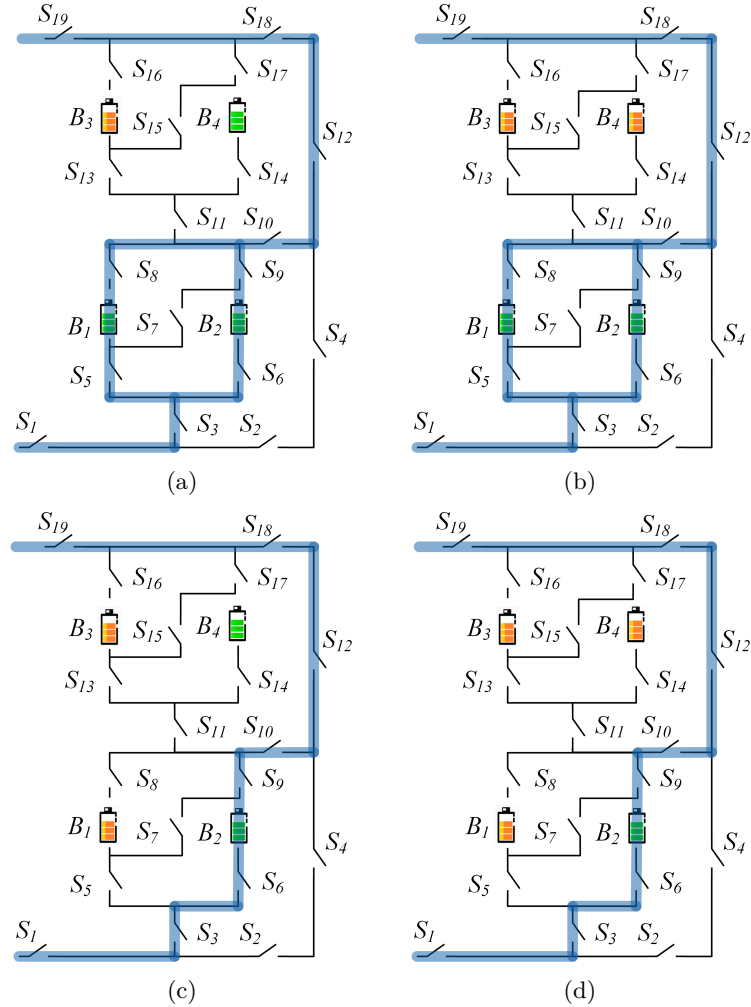


Figure 10: The circuit states of MACs when isolating (a) one, (b) two (in different substructures), (c) two (in the same substructure), and (d) three batteries for the structure in Fig. 4c.

332 **3.3 Discussion**

333 **3.3.1 Result validation**

334 The correctness of the outcomes provided by the proposed greedy algorithm will now be discussed
335 from two perspectives: circuit analysis and validation against the brute-force algorithm. The result
336 of the four-battery RBS structure shown in Fig. 4c is determined as an example. When B_1 and B_2
337 or B_3 and B_4 are connected in parallel, the RBS produces the maximum current, which is $\eta = 2$ (i.e.,
338 twice the current output of a single battery in the RBS). Adding more batteries to the main circuit
339 only creates a series structure and does not improve the MAC. Therefore, the switch-control scheme
340 provided in Tab. 4 maximizes the RBS output current. The brute-force method, which examines
341 all possible switch states, yields the same η . This indicates that the proposed greedy algorithm
342 successfully identifies the MAC among all the potential reconfigured structures.

343 **3.3.2 Pros and cons analysis**

344 The proposed greedy algorithm possesses a significant advantage in terms of its effectiveness and
345 efficiency. In this paper, it is compared with the brute-force algorithm, SA, and GA. While the
346 brute-force algorithm ensures the correctness of the results by exploring all possible switch states,
347 it comes at a high computational cost. The SA and GA are commonly used heuristic algorithms
348 for addressing NP-hard problems. They selectively generate solutions for the switching states to
349 maximize the objective value η . However, neither of these two algorithms can determine whether
350 the current η represents the final MAC or if there are better solutions. Moreover, as depicted in
351 Figs. 7a–7c and Figs. 9a–9b, the SA and GA algorithms require more iterations to converge to the
352 final solution than the proposed greedy algorithm.

353 To further elaborate on the efficiency of our algorithm, we analyze the time complexity of both
354 the brute-force algorithm and the greedy algorithm. If an RBS has N_b batteries and N_s switches and
355 the corresponding directed graph has N nodes, 2^{N_s} iterations are required to traverse all possible
356 structures. Calculating each reconfigured structure using Eqs. (7)–(10) requires matrix inversion
357 and matrix multiplication, which results in a time complexity of $O(N^3 + 2N^2N_b + N^2N_s + NN_b^2)$.
358 Therefore, the time complexity of the brute-force algorithm is $O((N^3 + 2N^2N_b + N^2N_s + NN_b^2)2^{N_s})$.
359 The greedy algorithm proposed in this paper requires that the SP be found for each battery, which
360 requires N_b iterations. Each SP can be obtained through several applications of Dijkstra's algorithms.
361 Therefore, the total time complexity for calculating all SPs is $O(N_b(N_b + 2N_s) \log_{10} N)$. According to
362 Appendix 1, the RBS can reconfigure $C_{N_b}^{N_{\text{set}}}$ structures by selecting N_{set} batteries from N_b batteries,
363 which gives $\sum_{N_{\text{set}}=1}^{N_b} C_{N_b}^{N_{\text{set}}} / N_b \approx 2^{N_b} N_b^{-1}$ on average. Thus, with the bisection method, the time
364 complexity of the greedy algorithm is $O((N^3 + 2N^2N_b + N^2N_s + NN_b^2)2^{N_b} N_b^{-1} \log_{10} N_b + N_b(N_b +$
365 $2N_s) \log_{10} N)$. For the existing RBS structures in the literature [39, 40, 41, 42, 43, 44], the number
366 of batteries N_b , the number of switches N_s , and the number of nodes N are quantitatively related
367 as follows: $N_s \approx (3-5)N_b$, $N \approx N_s$. After simplifying, the time complexity of the method with the
368 greedy algorithm is $O(2^{N_b} N_s^2 \log_{10} N_b)$, while that of the method with the brute-force algorithm is
369 $O(2^{N_s} N_s^3)$. Therefore, as the RBS grows, especially in terms of the number of switches, the greedy
370 algorithm gains an advantage over the brute-force algorithm. This is confirmed by the number of

371 structures required to determine the MAC in the previous section. Compared with the brute-force
372 algorithm, the method based on the greedy algorithm is 3 000 to 48 000 times more efficient, which
373 is theoretically $N_s 2^{N_s - N_b} \log_{10} N_b$ times according to the above time-complexity analysis. This is
374 the result of two key factors:

- 375 (1) The SPs guide the RBS to reconfigure reasonable structures rather than blindly going through
376 all possible structures. This reduces the complexity from 2^{N_s} to 2^{N_b} , which is the main reason
377 for the improvement in efficiency.
- 378 (2) The bisection method further accelerates this process, reducing the complexity from 2^{N_b} to
379 $2^{N_b} N_B^{-1} \log_{10} N_b$.

380 Furthermore, this approach can handle RBSs with arbitrary structures, which is another signif-
381 icant advantage. It can even do this when they have different battery variations or even random
382 isolated batteries. Theoretically, each RBS structure can be transformed into a unique directed
383 graph model using the methodology described in Section II, and the MAC can subsequently be
384 calculated using the proposed greedy algorithm. This finding is supported by the findings in the
385 previous subsection.

386 However, the suggested greedy algorithm still includes exponential terms in its time complexity,
387 indicating that it struggles to perform at scale. Additionally, all batteries are assumed to be identical
388 for the sake of simplification in the derivation. However, in reality, there may exist a small balancing
389 current that could introduce a minor bias in the MAC due to variations in the open-circuit voltage u_b
390 and the internal resistance r_b . Nevertheless, the proposed greedy algorithm remains a viable choice
391 for RBS design and optimization in the early stage, and the issue of balancing current bias can be
392 addressed by considering the inconsistency between batteries and replacing the internal resistance
393 with impedance when constructing the directed graph model.

394 3.3.3 Application scenarios

395 Note that η is used as the objective function instead of I_o in solving for the MAC. This choice makes
396 the resulting MAC more reasonable and applicable to practical scenarios. As shown in Tab. 4, I_o
397 and \mathbf{I}_b are functions of R_o , u_b , and r_b . However, when I_o is used as the objective function, even
398 for the same RBS structure, the MAC solution and corresponding switch states can change due
399 to different external electrical appliances. This increases the difficulty and uncertainty involved in
400 designing the RBS structure. To eliminate this problem, the ratio $\eta = I_o / \max(\mathbf{I}_b)$ is adopted as
401 the objective function in our research. Recall that η reflects only the structure's ability to output
402 current, rather than the actual current output by the battery system. Assuming that the MAC of
403 the batteries in the RBS is I_m , the maximum output current of the RBS structure can be calculated
404 as ηI_m by determining the value of η for the structure.

405 The method proposed in this paper facilitates the design of RBSs in the following ways. Most of
406 the existing RBS structures [39, 40, 41, 42, 43, 44] have simple topological characteristics, so calcu-
407 lating their MACs is relatively straightforward or even intuitive. However, these simple structures
408 do not always fully satisfy the requirements of complex applications, such as dynamically adapting

409 the circuit to variable and random operating conditions or actively equalizing differences between
410 batteries in the RBS. Moreover, isolating the batteries disrupts the original regularity and symmetry
411 of the topology, which complicates the otherwise simple structure, and the maximum output current
412 of the system becomes more challenging to obtain. In contrast, the proposed method calculates the
413 MAC of arbitrary RBS structures, most notably complex and flexible RBS structures.

414 To illustrate this point, the MACs of the RBS structure in Fig. 4c are calculated after isolating
415 one or more of the batteries, as shown in Figs. 10a–10d. When a single battery is isolated, the
416 RBS is still capable of outputting the maximum current, denoted as $\eta = 2$. When two batteries are
417 isolated, there are two scenarios: one is isolating two batteries within the same substructure (Fig.
418 10b), resulting in $\eta = 2$; the other is isolating one battery in each of the two substructures (Fig. 10c),
419 resulting in $\eta = 1$. If three batteries are isolated, the RBS can only output the current of a single
420 battery, which is $\eta = 1$. Therefore, the battery management system can adjust the output current
421 and control the RBS to reconfigure the corresponding structure based on the isolated batteries.

422 4 Conclusion

423 This paper has proposed a reliable and automated method to efficiently compute the MAC of an
424 RBS. The method is implemented using a greedy algorithm combined with an improved directed
425 graph model. Not only does the method provide the same global MAC calculation results as the
426 brute-force method, but it also demonstrates superior computational efficiency to both the brute-
427 force algorithm and the heuristic algorithms (SA and GA). Theoretically, for an RBS with N_s
428 switches and N_b batteries, the efficiency of the proposed method is $N_s 2^{N_s - N_b} \log_{10} N_b$ times that
429 of the brute-force method. This is primarily due to the utilization of the batteries' SPs guiding the
430 RBS to reconfigure reasonable structures rather than blindly going through all possible structures.
431 Another advantage of this method is its capability to calculate the MACs of RBSs with arbitrary
432 structures and varying batteries. Even in scenarios with random isolated batteries, the proposed
433 method remains effective. This method can facilitate the full utilization of the RBS's current output
434 potential, guide the design and optimization of the RBS structure, and assist in evaluating the risk
435 of current overload in practical applications.

436 5 Appendix

437 Acknowledgments

438 Author Contributions

439 B. Xu conceived the main idea, formulated the overarching research goals and aims, designed the
440 algorithm, and reviewed and revised the manuscript. G. Hua developed and analyzed the model,
441 implemented the code and supporting algorithms, and wrote the initial draft. C. Qian provided
442 critical review, commentary, and revisions. Q. Xia contributed to shaping the research, analysis,

Algorithm 1: Obtain the maximum available current (MAC) of a given RBS

Data: Directed graph model $G(V, E)$ of the RBS
Result: $\max \eta$

```

1 for  $i \in E_b$  do
2    $P_i \leftarrow \{path | \text{starts at } v_1 \text{ and ends at } v_n\};$ 
3    $SP_i \leftarrow p_i \text{ which has the minimum } \omega(p_i) \text{ among all } p_i \in P_i.$ 
4 end
5 Get  $\mathbf{A}$  by Eq. 1;
6 while not yet determined  $\max \eta$  do
7    $N_{\text{set}} \leftarrow$  number of selected SPs calculated by dichotomy;
8    $C_b \leftarrow$  set of all combinations of  $N_{\text{set}}$  batteries from  $N_b$ ;
9   for  $c_b \in C_b$  do
10     $\mathbf{x}_s \leftarrow$  list of all switches' states:  $x_s[j] = 1$  if  $j \in \bigcup_{i \in c_b} SP_i$  else 0;
11     $\mathbf{X} \leftarrow diag[1, 1, \dots, 1, \mathbf{x}_s];$ 
12    get  $\mathbf{Y}_n$  by Eq. 9;
13    if  $\mathbf{Y}_n$  is invertible then
14      | pass
15    else
16      | construct an effective solution
17    end
18    get  $I_o$  by Eq. 7;
19    get  $\mathbf{I}_b$  by Eq. 8;
20    if  $\max(\mathbf{I}_b) \leq I_m$  then
21      |  $\eta \leftarrow I_o / \max(\mathbf{I}_b);$ 
22    else
23      | break
24    end
25  end
26 end

```

443 and manuscript. B. Sun conducted the research and investigation process. Y. Ren secured the
444 funding and supervised the project. Z. Wang verified the results and provided necessary resources.

445 **Conflicts of Interest**

446 The authors declare that there is no conflict of interest regarding the publication of this article.

447 **Data Availability**

448 This work does not require any data to be declared or publicly disclosed.

449 **References**

- 450 [1] Yuqing Yang, Stephen Bremner, Chris Menictas, and Merlinde Kay. Battery energy storage
451 system size determination in renewable energy systems: A review. *Renewable and Sustainable
Energy Reviews*, 91:109–125, August 2018.
- 453 [2] Luanna Maria Silva de Siqueira and Wei Peng. Control strategy to smooth wind power output
454 using battery energy storage system: A review. *Journal of Energy Storage*, 35:102252, March
455 2021.
- 456 [3] Eugene Schwanbeck and Penni Dalton. International Space Station Lithium-ion Batteries for
457 Primary Electric Power System. In *2019 European Space Power Conference (ESPC)*, pages 1–1.
458 IEEE, September 2019.
- 459 [4] Lihua Zhang. Development and Prospect of Chinese Lunar Relay Communication Satellite.
460 *Space: Science & Technology*, 2021, January 2021.
- 461 [5] Jaephil Cho, Sookkyung Jeong, and Youngsik Kim. Commercial and research battery technologies
462 for electrical energy storage applications. *Progress in Energy and Combustion Science*,
463 48:84–101, June 2015.
- 464 [6] Naixing Yang, Xiongwen Zhang, BinBin Shang, and Guojun Li. Unbalanced discharging and
465 aging due to temperature differences among the cells in a lithium-ion battery pack with parallel
466 combination. *Journal of Power Sources*, 306:733–741, February 2016.
- 467 [7] Fei Feng, Xiaosong Hu, Lin Hu, Fengling Hu, Yang Li, and Lei Zhang. Propagation mechanisms
468 and diagnosis of parameter inconsistency within Li-Ion battery packs. *Renewable and
Sustainable Energy Reviews*, 112:102–113, September 2019.
- 470 [8] J. A. Jeevarajan and C. Winchester. Battery Safety Qualifications for Human Ratings. *Interface
magazine*, 21(2):51–55, January 2012.
- 472 [9] Daniel Vázquez Pombo. A Hybrid Power System for a Permanent Colony on Mars. *Space:
Science & Technology*, 2021, January 2021.

- 474 [10] Weiji Han, Torsten Wik, Anton Kersten, Guangzhong Dong, and Changfu Zou. Next-
475 Generation Battery Management Systems: Dynamic Reconfiguration. *IEEE Industrial Electronics Magazine*, 14(4):20–31, December 2020.
- 477 [11] Song Ci, Ni Lin, and Dalei Wu. Reconfigurable battery techniques and systems: A survey.
478 *IEEE Access*, 4:1175–1189, 2016.
- 479 [12] Nejmeddine Bouchhima, Matthias Gossen, Sascha Schulte, and Kai Peter Birke. Lifetime of
480 self-reconfigurable batteries compared with conventional batteries. *Journal of Energy Storage*,
481 15:400–407, 2018.
- 482 [13] Song Ci, Jiucai Zhang, Hamid Sharif, and Mahmoud Alahmad. A novel design of adap-
483 tive reconfigurable multicell battery for power-aware embedded networked sensing systems.
484 In *IEEE GLOBECOM 2007-IEEE Global Telecommunications Conference*, pages 1043–1047.
485 IEEE, 2007.
- 486 [14] Jan Engelhardt, Tatiana Gabderakhmanova, Gunnar Rohde, and Mattia Marinelli. Reconfig-
487 urable stationary battery with adaptive cell switching for electric vehicle fast-charging. In *2020*
488 *55th International Universities Power Engineering Conference (UPEC)*, pages 1–6, 2020.
- 489 [15] Jan Engelhardt, Jan Martin Zepter, Tatiana Gabderakhmanova, Gunnar Rohde, and Mattia
490 Marinelli. Double-string battery system with reconfigurable cell topology operated as a fast
491 charging station for electric vehicles. *Energies*, 14(9):2414, 2021.
- 492 [16] H. Visairo and P. Kumar. A reconfigurable battery pack for improving power conversion effi-
493 ciency in portable devices. In *2008 7th International Caribbean Conference on Devices, Circuits*
494 *and Systems*, pages 1–6. IEEE, April 2008.
- 495 [17] Barrie Lawson. A Software Configurable Battery. *EVS26 International Battery, Hybrid and*
496 *Fuel Cell Electric Vehicle Symposium*, pages 252–263, 2012.
- 497 [18] Liang He, Linghe Kong, Siyu Lin, Shaodong Ying, Yu Gu, Tian He, and Cong Liu.
498 Reconfiguration-assisted charging in large-scale lithium-ion battery systems. In *2014*
499 *ACM/IEEE International Conference on Cyber-Physical Systems (ICCPs)*, pages 60–71. IEEE,
500 2014.
- 501 [19] Hahnsang Kim and Kang G Shin. On dynamic reconfiguration of a large-scale battery system.
502 In *2009 15th IEEE Real-Time and Embedded Technology and Applications Symposium*, pages
503 87–96. IEEE, 2009.
- 504 [20] Weiji Han and Anton Kersten. Analysis and Estimation of the Maximum Circulating Current
505 during the Parallel Operation of Reconfigurable Battery Systems. In *2020 IEEE Transportation*
506 *Electrification Conference & Expo (ITEC)*, pages 229–234. IEEE, June 2020.
- 507 [21] Jan Engelhardt, Jan Martin Zepter, Tatiana Gabderakhmanova, Gunnar Rohde, and Mattia
508 Marinelli. Double-String Battery System with Reconfigurable Cell Topology Operated as a Fast
509 Charging Station for Electric Vehicles. *Energies*, 14(9):2414, 2021.

- 510 [22] Weiji Han, Anton Kersten, Changfu Zou, Torsten Wik, Xiaoliang Huang, and Guangzhong
 511 Dong. Analysis and estimation of the maximum switch current during battery system recon-
 512 figuration. *IEEE Transactions on Industrial Electronics*, 69(6):5931–5941, 2021.
- 513 [23] Lidiya Komsiyksa, Tobias Buchberger, Simon Diehl, Moritz Ehrensberger, Christian Hanzl,
 514 Christoph Hartmann, Markus Hözle, Jan Kleiner, Meinert Lewerenz, Bernhard Liebhart,
 515 Michael Schmid, Dominik Schneider, Sascha Speer, Julia Stöttner, Christoph Terbrack, Michael
 516 Hinterberger, and Christian Endisch. Critical Review of Intelligent Battery Systems: Chal-
 517 lenges, Implementation, and Potential for Electric Vehicles. *Energies*, 14(18):5989, 2021.
- 518 [24] Luis D. Couto and Michel Kinnaert. Partition-based Unscented Kalman Filter for Recon-
 519figurable Battery Pack State Estimation using an Electrochemical Model. In *2018 Annual
 520 American Control Conference (ACC)*, pages 3122–3128. IEEE, June 2018.
- 521 [25] Anton Kersten, Manuel Kuder, Weiji Han, Torbjorn Thiringer, Anton Lesnicar, Thomas Weyh,
 522 and Richard Eckerle. Online and On-Board Battery Impedance Estimation of Battery Cells,
 523 Modules or Packs in a Reconfigurable Battery System or Multilevel Inverter. In *IECON 2020
 524 The 46th Annual Conference of the IEEE Industrial Electronics Society*, pages 1884–1891. IEEE,
 525 October 2020.
- 526 [26] Michael Schmid, Emanuel Gebauer, Christian Hanzl, and Christian Endisch. Active Model-
 527 Based Fault Diagnosis in Reconfigurable Battery Systems. *IEEE Transactions on Power Elec-
 528 tronics*, 36(3):2584–2597, March 2021.
- 529 [27] Jan Kacel, Jingyang Fang, Tomas Kacel, Nima Tashakor, and Stefan Goetz. Design and
 530 Analysis of Modular Multilevel Reconfigurable Battery Converters for Variable Bus Voltage
 531 Powertrains. *IEEE Transactions on Power Electronics*, 38(1):130–142, January 2023.
- 532 [28] Feng Yang, Fei Gao, Baochang Liu, and Song Ci. An Adaptive Control Framework for Dynam-
 533 ically Reconfigurable Battery Systems Based on Deep Reinforcement Learning. *IEEE Transac-
 534 tions on Industrial Electronics*, 69(12):12980–12987, December 2022.
- 535 [29] Weiji Han, Changfu Zou, Liang Zhang, Quan Ouyang, and Torsten Wik. Near-Fastest Battery
 536 Balancing by Cell/Module Reconfiguration. *IEEE Transactions on Smart Grid*, 10(6):6954–
 537 6964, November 2019.
- 538 [30] Xinghua Liu, Guoyi Chang, Jiaqiang Tian, Zhongbao Wei, Xu Zhang, and Peng Wang. Flexible
 539 path planning-based reconfiguration strategy for maximum capacity utilization of battery pack.
 540 *Journal of Energy Chemistry*, 86:362–372, November 2023.
- 541 [31] Si-Zhe Chen, Yule Wang, Guidong Zhang, Le Chang, and Yun Zhang. Sneak Circuit Theory
 542 Based Approach to Avoiding Short-Circuit Paths in Reconfigurable Battery Systems. *IEEE
 543 Transactions on Industrial Electronics*, 68(12):12353–12363, 2021.
- 544 [32] Kailong Liu, Zhongbao Wei, Chenghui Zhang, Yunlong Shang, Remus Teodorescu, and Qing-
 545 Long Han. Towards Long Lifetime Battery: AI-Based Manufacturing and Management.
 546 *IEEE/CAA Journal of Automatica Sinica*, 9(7):1139–1165, July 2022.

- 547 [33] Morteza Mollajafari. An efficient lightweight algorithm for scheduling tasks onto dynamically
548 reconfigurable hardware using graph-oriented simulated annealing. *Neural Computing and Ap-*
549 *plications*, 35(24):18035–18057, August 2023.
- 550 [34] Liang He, Linghe Kong, Siyu Lin, Shaodong Ying, Yu Gu, Tian He, and Cong Liu. Reconfiguration-assisted charging in large-scale Lithium-ion battery systems. In *2014*
551 *ACM/IEEE International Conference on Cyber-Physical Systems (ICCPs)*, pages 60–71. IEEE,
552 April 2014.
- 554 [35] Zoltan Mark Pinter, Dimitrios Papageorgiou, Gunnar Rohde, Mattia Marinelli, and Chresten
555 Traholt. Review of Control Algorithms for Reconfigurable Battery Systems with an Industrial
556 Example. In *2021 56th International Universities Power Engineering Conference (UPEC)*,
557 pages 1–6, August 2021.
- 558 [36] Liang He, Lipeng Gu, Linghe Kong, Yu Gu, Cong Liu, and Tian He. Exploring Adaptive
559 Reconfiguration to Optimize Energy Efficiency in Large-Scale Battery Systems. In *2013 IEEE*
560 *34th Real-Time Systems Symposium*, pages 118–127, December 2013.
- 561 [37] Hongwen He, Rui Xiong, Xiaowei Zhang, Fengchun Sun, and JinXin Fan. State-of-Charge
562 Estimation of the Lithium-Ion Battery Using an Adaptive Extended Kalman Filter Based on
563 an Improved Thevenin Model. *IEEE Transactions on Vehicular Technology*, 60(4):1461–1469,
564 May 2011.
- 565 [38] S.M. Mousavi G. and M. Nikdel. Various battery models for various simulation studies and
566 applications. *Renewable and Sustainable Energy Reviews*, 32:477–485, April 2014.
- 567 [39] Song Ci, Jiucai Zhang, Hamid Sharif, and Mahmoud Alahmad. A Novel Design of Adaptive
568 Reconfigurable Multicell Battery for Power-Aware Embedded Networked Sensing Systems. In
569 *IEEE GLOBECOM 2007-2007 IEEE Global Telecommunications Conference*, pages 1043–1047,
570 November 2007.
- 571 [40] Mahmoud Alahmad, Herb Hess, Mohammad Mojarradi, William West, and Jay Whitacre. Bat-
572 tery switch array system with application for JPL’s rechargeable micro-scale batteries. *Journal*
573 *of Power Sources*, 177(2):566–578, March 2008.
- 574 [41] Hahnsang Kim and Kang G. Shin. Dependable, efficient, scalable architecture for management
575 of large-scale batteries. In *Proceedings of the 1st ACM/IEEE International Conference on Cyber-*
576 *Physical Systems*, ICCPS ’10, pages 178–187, New York, NY, USA, April 2010. Association for
577 Computing Machinery.
- 578 [42] Younghyun Kim, Sangyoung Park, Yanzhi Wang, Qing Xie, Naehyuck Chang, Massimo Pon-
579 cino, and Massoud Pedram. Balanced reconfiguration of storage banks in a hybrid electrical
580 energy storage system. In *2011 IEEE/ACM International Conference on Computer-Aided De-*
581 *sign (ICCAD)*, pages 624–631, November 2011.

- 582 [43] Taesic Kim, Wei Qiao, and Liyan Qu. A series-connected self-reconfigurable multicell battery
583 capable of safe and effective charging/discharging and balancing operations. In *2012 Twenty-*
584 *Seventh Annual IEEE Applied Power Electronics Conference and Exposition (APEC)*, pages
585 2259–2264, February 2012.
- 586 [44] Liang He, Linghe Kong, Siyu Lin, Shaodong Ying, Yu Gu, Tian He, and Cong Liu.
587 Reconfiguration-assisted charging in large-scale Lithium-ion battery systems. In *2014*
588 *ACM/IEEE International Conference on Cyber-Physical Systems (ICCPs)*, pages 60–71, April
589 2014.

